

DISCLAIMER

This report was prepared as an account of work sponsored by an agency of the United States Government. Neither the United States Government nor any agency thereof, nor any of their employees, makes any warranty, express or implied, or assumes any legal liability or responsibility for the accuracy, completeness, or usefulness of any information, apparatus, product, or process disclosed, or represents that its use would not infringe privately owned rights. Reference herein to any specific commercial product, process, or service by trade name, trademark, manufacturer, or otherwise does not necessarily constitute or imply its endorsement, recommendation, or favoring by the United States Government or any agency thereof. The views and opinions of authors expressed herein do not necessarily state or reflect those of the United States Government or any agency thereof.

This report has been reproduced directly from the best available copy.

Available to DOE and DOE contractors from the Office of Scientific and Technical Information, P.O. Box 62, Oak Ridge, TN 37831; prices available from (615)576-8401, FTS 626-8401.

Available to the public from the National Technical Information Service, U.S. Department of Commerce, 5285 Port Royal Rd., Springfield, VA 22161.

Fundamentals of Foam Transport
in Porous Media

Topical Report

By
A.R. Kavscek
C.J. Radke

October 1993

Prepared for
U.S. Department of Energy
Assistant Secretary for Fossil Energy

Thomas B. Reid, Project Manager
Bartlesville Project Office
P.O. Box 1398
Bartlesville, OK 74005

Prepared by
Earth Sciences Division of
Lawrence Berkeley Laboratory
and
Department of Chemical Engineering
University of California, Berkeley
Berkeley, CA 94720

Table of Contents

Abstract	v
Introduction	1
Foam Microstructure	4
Foam Transport	6
Effective Permeability	6
Effective Viscosity	9
Synopsis	12
Mechanisms of Foam Formation and Decay	13
Foam Formation	13
Foam Destruction	16
Foam Flow at Limiting Capillary Pressure	22
Population-Balance Modeling of Foam Flow in Porous Media	24
Conservation Equations	25
Generation	27
Coalescence	29
Gas Mobility	31
Making and Breaking	34
Experiment	35
Comparison of Theory and Experiment	36
Model Parameters	36
Transient Displacement	38
Steady Behavior	40
Summary	41
Acknowledgement	44
Literature Cited	46
Table 1: Parameter Values	53
Figure Captions	54

Fundamentals of Foam Transport in Porous Media

A. R. Kavscek and C. J. Radke
Earth Sciences Division of Lawrence Berkeley Laboratory
and Department of Chemical Engineering
University of California, Berkeley
Berkeley, CA 94720 USA

Abstract

Foam in porous media is a fascinating fluid both because of its unique microstructure and because its dramatic influence on the flow of gas and liquid. A wealth of information is now compiled in the literature describing foam generation, destruction, and transport mechanisms. Yet there are conflicting views of these mechanisms and on the macroscopic results they produce. By critically reviewing how surfactant formulation and porous media topology conspire to control foam texture and flow resistance, we attempt to unify the disparate viewpoints.

Evolution of texture during foam displacement is quantified by a population balance on bubble concentration, which is designed specifically for convenient incorporation into a standard reservoir simulator. Theories for the dominant bubble generation and coalescence mechanisms provide physically based rate expressions for the proposed population balance. Stone-type relative permeability functions along with the texture-sensitive and shear-thinning nature of confined foam complete the model. Quite good agreement is found between theory and new experiments for transient foam displacement in linear cores.

Introduction

The mobilities of continuous, Newtonian fluids in reservoir media are inversely proportional to their viscosities. Thus, gas drive fluids for enhanced oil recovery, such as dense carbon dioxide, enriched hydrocarbons, nitrogen, and steam, are highly mobile causing them to channel selectively through zones of high permeability rather than efficiently displace oil. Further, gas drive fluids are also less dense than both brine and crude oil. They rise to the top of the reservoir and override the oil-rich zones. Traditional gas-displacement processes lack mobility control and result in poor volumetric displacement efficiency due to both channeling and gravity override.

In 1961, Fried (1) demonstrated that aqueous-surfactant-stabilized foam could drastically reduce the mobility of gases in porous media. At that time foam was studied mainly from a phenomenological perspective. In the intervening 30 years, foam has been recognized as a fluid with unique rheological properties within porous media, and the scope of research has expanded to include local pore-scale phenomena and local microstructure. Because of its dispersed nature, foam profoundly affects the flow patterns of nonwetting fluids within porous media.

In this chapter, we discuss much of the work accomplished since Fried, but without attempting a complete review. Useful synopses are available in the articles and reports of Hirasaki (2,3), Marsden (4), Heller and Kuntamukkula (5), Baghidikian and Handy (6), and Rossen (7). Our goals are to present a unified perspective of foam flow in porous media, to delineate important pore-level foam generation, coalescence, and transport mechanisms, and to propose a readily applicable one-dimensional mechanistic model for transient foam displacement based upon gas-bubble size evolution (i.e., bubble or lamella population balance (8,9)). Because foam microstructure or texture (i.e., the size of individual foam bubbles) has important effects on flow phenomena in porous media, it is mandatory that foam texture be accounted for in understanding foam transport.

Our discussion follows the goals listed above. First, we describe how foam is configured within porous media and how this configuration controls foam transport. Next, we review briefly pertinent foam generation and coalescence mechanisms. Finally, we incorporate pore-level microstructure and texture-controlling mechanisms into a population balance to model foam flow in porous media consistent with current reservoir-simulation practice (c.f., [10](#)). Attention is focused on completely water-wet media that are oil free. Interaction of foam with oil is deferred to Chapter 4.

Foam Microstructure

As we learned in Chapter 1, foam is a gas phase dispersed within a liquid phase and stabilized by surfactant adsorbed at the gas/liquid interface. In reservoir applications, foams are usually formed by nonwetting gases, such as steam or nitrogen, dispersed within a continuous, wetting aqueous phase containing surface-active agents. Foams formed with dense CO₂ as the internal phase are strictly emulsions, which led Wellington to coin the phrase "foamulsion" ([5](#)). We retain the term foam here. Some nonaqueous foams in porous media have been studied primarily for use as barriers against gas coning through thin oil zones ([11,12](#)) and well stimulation ([13,14](#)). However, since the basic principles appear similar, our discussion is limited to aqueous foams.

The behavior of foam in porous media is intimately related to the connectivity and geometry of the medium in which it resides. Porous media have several attributes which are important to foam flow. First, they are characterized by a size distribution of pore bodies (sometimes called pores) interconnected through pore throats of another size distribution. While the body and throat size distributions are important, as important is their possible correlation to give the distribution of body-to-throat size ratios. Foam generation and destruction mechanisms in porous media depend strongly on the body-to-throat size aspect ratio. Second, pores are not cylindrical but exhibit corners, as illustrated in Figure 1. Under two-phase occupancy one fluid preferentially wets the pore walls. The wetting fluid completely fills the smallest pores, and, resides in the corners of

gas-occupied pores and in thin wetting films coating pore walls. Because of the thin films, liquid in the corners of adjacent pores is contiguous with wetting liquid in the smallest pore space. Hence, the wetting phase remains continuous even down to very low saturations. The nonwetting phase resides in the central portion of the largest pores. Accordingly, Figure 1 portrays multiple phases jointly occupying the largest pores. Finally, at the pore level when flow rates are low and tension forces dominate (i.e., for Bond and capillary numbers much less than unity), the capillary pressure is constant set by the local saturation of the wetting phase and the value of the interfacial tension. Local imbalances in capillary pressure tend to equalize primarily through the interlinked, continuous wetting phase. Local capillary-pressure information is transmitted to foam lamellae and/or lenses in the same manner. During biphasic flow of continuum fluids, the nonwetting fluid flows in interconnected large pore channels. Wetting fluid flows in interconnected small pore channels and in the corners and thin films of the nonwetting-phase occupied pores due to pressure gradients in the aqueous phase and viscous traction at the contacting interface.

The morphology and mechanisms of foam flow in porous media are not nearly so clear. They have been scrutinized since the earliest studies (1,15). Even at small Reynolds numbers at least four microstructure regimes may be envisioned. When the characteristic length scale of the pore space is much greater than the size of individual foam bubbles, the foam is properly designated as bulk. Bulk foam is further divided into kugelschaum ("ball foam") and polyderschaum ("polyhedral foam") (16). The former consists of well-separated, spherical bubbles while the latter consists of polyhedral bubbles separated by surfactant-stabilized, thin-liquid films called lamellae. The distinguishing feature is the fraction of foam volume that is gas or the foam quality. High gas fractions correspond to polyderschaum and *vice versa*. Bulk foam is discussed further in Chapter 2; the flow of bulk foam outside porous media is reviewed by Kraynik (17).

Conversely, when the characteristic pore size of the medium is comparable or less than the characteristic size of the dispersed gas bubbles, the bubbles and lamellae span completely across pores (18). We designate this regime as confined foam. Again, it is possible to distinguish two regimes of morphology based on the gas content of the foam. However, in-situ foam quality here

is not well defined. It is preferable to classify the two regimes according to gas fractional flow. Almost all researchers studying foam in porous media use quality to represent fractional flow. We also follow this convention. At low gas fractional flow the pore-spanning bubbles are widely spaced separated by thick wetting liquid lenses or bridges. Conversely, at high gas fractional flow the pore-spanning bubbles are in direct contact, separated by lamellae. Hirasaki and Lawson denote this latter morphology as the individual-lamellae regime (18). Since most foam-displacement applications in reservoir media utilize reasonably high gas fractional flows where the gas/aqueous-phase capillary pressure is high, bulk polyhedral foam or confined, individual-lamellae foam are the two most pertinent textures.

Marsden et al. (19) were apparently the first to determine the relevant size scale characteristic of foam in porous media. They measured mean bubble sizes for foam exiting sandpacks and concluded that foam bubbles were roughly the same size as pore bodies. Despite the equivalence of bubble and pore sizes they treated foam as a continuum, nonNewtonian fluid (i.e., a bulk foam). Holm (15), at roughly the same time, injected pregenerated foam into sandpacks and measured effluent bubble sizes. He noted effluent steady-state bubble diameters larger (0.6 mm) than average sand grain size (roughly 0.1 mm) and also larger than the injected bubble diameter (0.4 mm) for a foam of 90% quality and unspecified flow rates. Additionally, he concluded that under steady state conditions no free gas was present in the medium.

More recently, Ettinger and Radke (20,21) measured steady state effluent bubble size distributions exiting 0.5 to 1.0 μm^2 Berea sandstones and found average bubble sizes to be roughly twice as large as pore dimensions. Bubble diameters ranged from 0.05 to 0.7 mm depending upon the permeability of the sandstone and the gas and liquid injection rates. Average pore body size in similar Berea sandstones is roughly 0.18 mm (22). Ettinger and Radke confirm the finding of Holm (15) that pregenerated foam is reshaped by the porous medium. Further, Trienan et al. (23) found bubbles exiting sandpacks to be roughly 10 times larger than typical pore size at flow rates close to 1 m/day. Because effluent bubble sizes equal to or larger than pore

dimensions are universally reported, it is now generally accepted that single bubbles and lamellae span the pore space of most porous media undergoing foam flow.

Direct observation of foam in transparent etched-glass micromodels confirms that foam bubbles and lamellae generally span entire pores (24-26). A photomicrograph of a foam-filled micromodel (27) is shown in Figure 2. The lightest portions represent the rock matrix. Light gray shading corresponds to the wetting aqueous surfactant solution. The most darkly shaded portions indicate gas. Most importantly, note the dark pore-spanning lamellae that terminate in so-called Plateau borders adjacent to the pore walls. A white marker in the lower left of Figure 2 corresponds to a scale of 0.1 mm. Clearly the foam in Figure 2 is not bulk. Note also that the foam does not enter the large water-filled pore indicated by the black arrow because gas can not enter the barely visible small pore throat just below it. In spite of the dispersed state of the gas, it remains the nonwetting phase. Finally, note the cushions of wetting aqueous liquid residing next to the walls in the gas-occupied pores of Figure 2. These correspond to the wetting corner liquid pictured in Figure 1.

Figure 2 illustrates what is coined a discontinuous-gas foam (2,9) in that the entire gas phase is made discontinuous by lamellae, and there are no gas channels which are continuous over sample-spanning dimensions. Gas is encapsulated in small packets or bubbles by surfactant-stabilized aqueous films. These packets transport in a time averaged sense through the porous medium (20).

Not all confined foams are discontinuous (9). A "continuous-gas foam" is illustrated schematically in Figure 3. Here rock grains are hatched; gray shading represents gas trapped by stationary lamellae, shown as thick dark lines. A continuous gas channel is pictured unshaded. In continuous-gas foam the medium contains one or several interconnected gas channels that are uninterrupted by lamellae over macroscopic distances. As in discontinuous-gas confined foam, the wetting aqueous phase again fills the smallest pores (not shown in Figure 3). Continuous-gas foams (9) have been observed in beadpacks constructed from 0.6 to 0.8 mm sintered glass beads. Further evidence of continuous-gas foam is provided by Hanssen (11, 28, 29).

Typically, a discontinuous-gas foam forms under conditions of coinjection of wetting surfactant solution and gas where ample wetting phase is present and available for foam-generation events. Continuous-gas foams can form when the wetting-phase saturation falls sufficiently low so that significant lamella generation ceases, such as in the later stages of gas injection. Continuous-gas channels result. Nevertheless, stationary lamellae and bubbles remain and block gas transport (c.f., Figure 3) through the remaining portions of the pore network (9, 11). Gas mobility is still greatly reduced.

Foam Transport

The basic morphology of confined foam in porous media shown in Figures 2 and 3 suggests that gas mobility appearing in Darcy's law may be conceptually divided into effects on the gas permeability and viscosity. Because foam in porous media is strictly a nonlinear fluid, this separation may not be formally rigorous (5, 30). Nevertheless, this idea seems necessary to make progress toward modeling foam flow. Thus, stationary gas is equivalent to lowering the gas effective permeability while allowing gas flow in the open channels. Conversely, bubbles flowing in interconnected channels contribute extra resistance to transport that is best described by an effective gas viscosity.

Effective Permeability

Bernard and Holm (31) and Bernard et al. (32) pursued pioneering studies quantifying gas and liquid permeabilities in the presence of foam. They either coinjected surfactant solution and nitrogen or used alternating slugs of each. For consolidated porous media with absolute permeabilities ranging from 0.1 to 0.25 μm^2 they found several-hundred-fold permeability reductions to gas. For a sandpack with an absolute permeability of 3.89 μm^2 , gas permeability was reduced to less than 10^{-3} μm^2 in the presence of foam.

Two important experimental observations were made at this early stage. Bernard et al. (32) varied aqueous-phase flow rates, and measured aqueous saturations and overall pressure drops.

Water relative permeabilities calculated with Darcy's law were surprisingly unaffected by foam. When compared under identical flow-rate conditions, steady-state water saturations were different between foam and surfactant-free, two-phase flow cases but the aqueous-phase relative permeability, k_{rw} , versus aqueous saturation, S_w , relation was unchanged. Since the wetting aqueous phase is primarily concentrated in small pores, it is unaffected by the dispersed nature of the nonwetting phase at any given saturation (c.f., Figure 2). Subsequently, the independence of the wetting-phase relative permeability on the presence of foam has been reconfirmed numerous times (15, 33-36).

Secondly, after foam flooding cores, Bernard et al. (32) flushed with water or brine to estimate trapped-gas saturation. They assumed that water or brine filled the pore space through which gas flowed, but did not substantially alter the fraction of gas trapped. Their trapped saturations ranged from 10 to 70 % depending upon the surfactant type and the presence of oil in the porous medium during the foam flood. Such measured saturations apply only to trapped gas following a waterflood, and not to dynamic or steady-state foam flooding.

Our knowledge of foam trapping remains incomplete. Gas-phase tracer experiments, however, measure trapped gas saturation of foams at steady state. Nahid, apparently, employed the technique first (37). More recently, gas-phase tracer experiments have revealed trapped gas saturations for nitrogen foams at steady state in Berea sandstones ranging from roughly 80% to nearly 100% over a variety of flow rates (38, 39). Friedmann et al. (39) used a krypton tracer for a range of frontal advance rates between 25 and 130 m/day. They measured the fraction of gas trapped as a function of gas-phase velocity at constant fractional flow. Interestingly, they found little change in the fraction trapped (approximately 85%) even though they varied the gas velocity by over two orders of magnitude. To correct for partitioning of the tracer into the trapped fraction Gillis and Radke (38) used sulfur hexafluoride and methane tracers simultaneously. Total flow rates ranged from 0.5 to 4 m/day. They also reported no consistent trend of trapped fraction with liquid or gas velocity. Remarkably, even when only gas was injected into a Berea sandstone at

connate saturation of aqueous surfactant solution, an appreciable fraction of the gas (in excess of 70 %) remained trapped. A continuous-gas foam was likely operative under these conditions.

Flumerfelt and Prieditis (40) performed a similar gas-only injection into a $7 \mu\text{m}^2$ beadpack. They first generated foam under conditions of simultaneous injection of gas and surfactant solution at a variety of gas rates but at fixed liquid rates. After reaching steady state, liquid flow was discontinued and the foam allowed to decay until continuous gas was produced. They showed that the permeability of the beadpack to gas at the first appearance of effluent continuous gas was two orders of magnitude less than the foam-free case and that this permeability was independent of gas and initial liquid flow rates. They concluded that the number of channels available to carry gas was 100 times less in the presence of foam than in the foam-free case.

These macroscopic measurements of gas trapping are confirmed by visual observations in transparent etched-glass micromodels and beadpacks (24-26,41). Trapped foam severely reduces the effective permeability of gas moving through a porous medium by blocking all but the least resistive flow paths. Hence, trapped gas reduces the void volume of the porous medium available for flow. Thus, higher flow resistances are measured, and lower permeabilities to gas are computed. This trapped gas accounts for some, but not all, increased resistance to flow.

Visual observation in etched-glass micromodels (26) additionally shows that foam trapping is an intermittent process. At steady state, only a portion of the foam flows during any moment. Primary channels known as backbone channels carry the major portion of flowing gas. These are relatively few in number. Leading off of the backbone channels are secondary or dendritic channels. None of these channels are always open to flow or blocked at all times. Sporadically, a series or train of foam bubbles mobilizes and flow begins. The identity of the individual bubbles in the series is constantly changing. Bubbles may join or leave the series, and individual lamellae may be broken or generated. Later, this series of bubbles may cease flowing and block a channel because of a switch in the flow path. The primary characteristic of porous media which permits this switching of flow paths is a high degree of interconnectedness. It is clear that in both continuous

and discontinuous foam, trapped gas constitutes the majority of the gas volume in the medium and must be accounted for in any modeling effort.

On a theoretical level, foam mobilization and trapping is perhaps best tackled with percolation models. Such models (42-47), coupled with micromodel visualization, support the above mechanistic view of foam trapping. Results indicate that the pressure gradients required to maintain foam flow are quite high on the order of 2 to over 200 kPa/m (1 to 10 psi/ft) (42-44). Rossen suggests that the ease of initiating flow increases with the degree of interconnectedness and lower interfacial tension, but decreases with gas compressibility (45). The most important factors affecting bubble trapping are pressure gradient, gas velocity, pore geometry, foam texture, and bubble-train length (42).

Effective Viscosity

There is considerable evidence that in some gas-occupied channels confined foam bubbles transport as bubble trains. Effluent bubble sizes from 0.8 μm^2 Berea sandstone reflect expected sizes and their predicted shift with flow velocity (20). Likewise, pregenerated foam is reshaped to the same average exiting size quite independent of the average inlet size (20). As with trapped foam, there is ample direct visual documentation of flowing foam bubble trains in both micromodels (26) and in beadpacks (9,48). The flow resistance of transporting bubble trains is best addressed in terms of an effective gas viscosity.

Initially several researchers measured the effective viscosity of bulk foam using rotational or capillary viscometers (1,49) hoping to apply their results to porous media. Based on our earlier discussion of foam morphology in porous media, such data are inappropriate (50). Interaction of elongated bubbles and pore-spanning lamellae with pore walls determines the effective viscosity of the flowing portion of foam. Such interactions are simply not mirrored in bulk foam viscometry.

Bretherton provided the cornerstone study for understanding the effective viscosity of confined foam (51). He generated long surfactant-free gas bubbles and flowed them through small, liquid-filled, cylindrical capillary tubes such that the bubbles completely spanned the capillary diameter. The experiments demonstrated that for strongly liquid wet capillaries, a thin liquid film

deposits on the capillary wall. Film thickness increases with increasing bubble velocity, U . From a theoretical hydrodynamic analysis, Bretherton established that such bubbles indeed slide over a constant thickness film. The film thickness divided by tube radius scales as $Ca^{2/3}$ where $Ca = \mu U / \sigma$ is the capillary number for a liquid of viscosity, μ , and equilibrium surface tension, σ . Over the range $10^{-6} < Ca < 10^{-2}$ where inertia is unimportant, Bretherton's theory and experiments are in satisfactory agreement (51). Additionally, the pressure drop to drive a single bubble nondimensionalized by the ratio of surface tension to tube radius varies as $Ca^{2/3}$. As a result, the effective viscosity of an elongated, inviscid gas bubble, defined from Poiseuille flow, has an inverse 1/3 dependence on bubble velocity and at low capillary numbers is actually larger than that of an equivalent volume of liquid. The reason is that the shear rate of the liquid in the thin films near the front and back of the bubble is larger than that for simple parabolic flow of the liquid phase. Recently, Wong (52) extended the Bretherton analysis to square tubes to consider the role of pore corners noted in Figure 1. Aside from detailed differences in the nature of the thin wetting films deposited on the flat portions of the tube walls, the pressure drop to drive the bubble again scales as $Ca^{2/3}$. Straight, cornered pores still obey Bretherton's basic theory but with somewhat different scaling constants.

Hirasaki and Lawson (18) studied elongated bubble and lamella trains in aqueous surfactant solutions flowing through cylindrical capillaries. Their work provides important insight into the effective or apparent viscosity of foam in porous media. Surfactants play a role in bubble transport whenever they are limited by mass transfer or sorption kinetics from maintaining a constant equilibrium tension around the bubble. During flow, the front bubble interface stretches toward the capillary wall and the rear interface contracts toward the capillary centerline. Accordingly, surfactant depletes at the bubble front leading to a surface tension above the bulk equilibrium value, whereas surfactant accumulates at the bubble rear leading to a surface tension below the equilibrium value. A surface-tension gradient arises which is directed towards the bubble front and retards bubble motion. Hirasaki and Lawson demonstrate theoretically and experimentally that such

surfactant effects are important (18). Neglecting the surface-tension gradient underestimated effective viscosity by a factor of 8 (where $0.05 < U < 7$ cm/s).

Consideration of flowing bubble trains separated by lamellae leads to the important finding that, except for very short bubbles and very slow sorption kinetics, the effective viscosity of confined foam scales quite linearly with bubble density and, in concert with Bretherton, inversely proportional to the capillary number raised to the 1/3 power. The proportionality constant is a strong function of surfactant properties. The result is that flowing, confined foam is shear thinning, an observation first noted by Fried(1), and that finer textured foam (i.e., larger bubble or lamellae densities) causes larger flow resistance. We utilize these ideas in our later modeling effort.

Two notable approaches have been used to include the role of pore constrictions in the pressure gradient required to drive lamellae through constricted porous media. Falls et al. (48) added a viscous resistance accounting for pore constrictions that acts in series with the straight-tube flow resistance of Hirasaki and Lawson (18). Prieditis (41) and Rossen (42-44,46) computed the static curvature resistance to the movement of single and trains of bubbles through a variety of constricted geometries. Rossen considers the role of bubble compressibility (43), asymmetric lamella shapes (44), and stationary lamellae (46) on foam mobilization.

Interestingly, the two analyses are at odds. Lamella stretching is a dynamic effect and is not included in static arguments. Prieditis (41) argues that, as a lamella moves through a serially diverging and converging pore space, the energy used to stretch the lamella and allow it to flow through the diverging section is completely recovered as the lamella squeezes to move through the converging section. Falls et al. (48) believe the opposite. Energy is consumed both by viscous resistance to lamellae flow and by nearby stationary lamellae that oscillate in response to pressure fluctuations of the flowing portion of the foam. Notwithstanding viscous dissipation in nearby oscillating lamellae, the static energy to squeeze a lamella through a constricted pore must mostly be dissipated through an increased local velocity upon entering the pore throat. Thus, inclusion of pore constrictions and even pore corners does not alter the basic shear-thinning and texture-dependent behavior of flowing, confined foam.

Synopsis

Based on the preceding information, Radke and Gillis (38) proposed Figure 4 as a summary of the pore-level microstructure of foam during flow through porous media. Figure 4 applies specifically to a confined, discontinuous-gas foam in the individual-lamellae regime. In this highly schematic picture, hatched circles reflect water-wet sand grains. Wetting fluid is shown as the dotted phase. Foam bubbles are either unshaded or shaded gray to indicate whether they are flowing or trapped, respectively. Purely for illustrative purposes, the largest pore channels lie near the top of the picture while intermediate and smaller sized pores are located sequentially nearer to the bottom.

Because of the dominance of capillary forces, wetting surfactant solution flows as a separate phase in the smallest pore spaces. Minimal wetting liquid transports as lamellae. Accordingly, the wetting-phase relative permeability function is unchanged in the presence of foam. Flowing foam transports in the largest pores where it encounters the smallest flow resistance relative to other possible flow paths. Because the smallest pore channels are occupied solely by wetting liquid and the largest pore channels carry flowing foam, bubble trapping occurs in the intermediate-sized pores. If we refer to foam as a "phase", the flowing portion of the foam phase is most nonwetting while the trapped portion of the foam phase is of intermediate wettability. Thus, following the reasoning behind Stone-type models (53), the relative permeability function of the nonwetting flowing foam, and that of the flowing wetting phase, is unaffected by the presence of the intermediate-wettability phase. Flowing-foam relative permeability becomes solely a function of the gas saturation of flowing bubbles, and is much reduced by the trapped foam saturation. Of course, the relative permeability of the intermediate-wettability trapped foam is zero.

Foam bubbles moving in the largest backbone channels are coupled together through lamellae and lenses. They parade in series as trains. Individual bubbles comprising these trains are relentlessly destroyed and recreated, so that the train is in a constant state of rearrangement.

Regardless of whether bubbles are generated externally or in-situ, they are molded and reshaped by the porous medium (20, 26). Bubbles and lamellae transport some distance, perhaps through several pore bodies and throats, are destroyed, and then reformed. Further, trains halt when the local pressure gradient is insufficient to keep them mobilized, and other trains lurch into motion. The identity of a single bubble or train is not conserved over any large distance. Bubble trains exist only in a time-averaged sense.

Continuous-gas foams are readily accommodated within the above picture. During the later stages of gas-only injection, flowing lamellae may collapse and not be regenerated. Thus, some or all of the flowing bubble trains are replaced by continuous gas. Trapped lamellae then become mainly responsible for increased flow resistance. Confined, continuous-gas foam may be viewed as a subcase of discontinuous-gas foam.

Mechanisms of Foam Formation and Decay

Foam texture in Figures 2 through 4 arises because of strong lamella generation and coalescence forces. It is the interplay of bubble generation and coalescence which determines foam microstructure and, hence, gas mobility in porous media. Knowledge of these pore-level events is necessary to derive physically meaningful rate expressions for foam generation and coalescence. We follow closely, although in much less detail, the exposition of Chambers and Radke (26) who provide visual documentation of and explanations for the various mechanisms.

Foam Formation

Three fundamental pore-level generation mechanisms exist: snap-off, division, and leave-behind. We briefly discuss each in turn.

Snap-off is a very significant mechanism for bubble generation in porous media. This phenomenon was first identified and explained by Roof (54) to understand the origin of residual oil. Snap-off is not restricted to the creation of trapped oil globules. It repeatedly occurs during

multiphase flow in porous media regardless of the presence or absence of surfactant. Hence, snap-off is recognized as a mechanical process.

Figure 5a illustrates a gas finger entering a pore constriction initially filled with wetting liquid. The pore is considered cornered in cross-section with local transverse inscribed radius R_C . Upon reaching the throat, the interface curvature and corresponding capillary pressure rise to the equilibrium entry value. As the bubble front enters the downstream body, wetting liquid remains in the corners (cf., Figure 1), and the curvature and corresponding local capillary pressure at the bubble front fall with expansion of the interface. The resulting gradient in capillary pressure initiates a gradient in liquid pressure directed from the pore body toward the pore throat. Liquid is driven along the corners into the pore throat where it accumulates as a collar (Figure 5b). Close examination of Figure 2 also reveals such a collar demarked with the black arrow just right of center. Collar growth to snap-off ensues in Figure 5c provided that the downstream bubble front has a mean radius of curvature that is larger than about twice R_C and provided that the constriction is not extremely sharp. If the constriction is too sharp, a stable collar can form. Thus, snap-off or germination sites (26) in porous media must exhibit a body-to-throat size aspect ratio larger than about two and be gently sloped. They also require sufficient wetting liquid. Snap-off creates gas bubbles that are approximately the size of pore bodies.

The growth wavelength of the unstable collar in Figure 5 is close to $2\pi R_C$ which means that snap-off always creates a lens (Figure 5c). It is not possible to generate a lamella directly at a pore throat by snap-off. Chambers and Radke point out that lamellae form downstream of the constriction as a newly formed bubble bumps into other previously created bubbles (cf., Figures 19 and 20 of (26)). If stabilizing surfactant is not present in the wetting phase, snapped off bubbles quickly coalesce (26,45,55) so that on the average continuous gas channels exist. Snap-off followed by coalescence events is a standard ingredient of multiphase flow.

Three varieties of snap-off exist depending upon whether local liquid saturation is increasing or decreasing and upon the pore-body to pore-throat aspect ratio (26). Figure 5 portrays neck or Roof snap-off, which is most prevalent at high wetting liquid saturations. Rectilinear and

pre-neck constriction snap-off contribute when both phases are flowing near steady state at lower wetting liquid saturations. Pre-neck snap-off occurs when a gas bubble lodges upstream of a pore throat and blocks liquid flow causing a deformation in the gas/liquid interface. Depending on the detailed geometry of the pore, snap-off ensues when an adequate amount of liquid accumulates (26). Rectilinear snap-off occurs in long ($\text{length} > 2\pi R_T$) straight pores in a fashion akin to snap-off in straight, cornered capillary tubes. In all three types of snap-off a wetting liquid lens forms first. Also, all three types occur regardless of the presence of surfactant. Snap-off depends on liquid saturation or, equivalently, on the medium capillary pressure, in addition to pore geometry, and wettability (56-58), but, except for altering solution properties such as surface tension, is sensibly independent of surfactant formulation.

Lamella or bubble division proceeds by subdividing foam bubbles or lamellae. Thus, mobile foam bubbles must pre-exist. Division is illustrated in Figure 6. A translating foam bubble encounters a point where flow branches in two directions (Figure 6a). The interface stretches around the branch point and enters both flow paths. The initial bubble divides into two separate bubbles (Figure 6b) that continue moving downstream.

Whether or not a lamella divides is governed by several factors. First, Chambers (27) has observed that foam bubbles which are smaller than the pore-body size do not divide when they encounter a branch point. The bubble flows down one or the other of the channels unaltered. If, however, the bubble size is larger than that of the pore body so that the foam lamella spans the pore space, division generally occurs. Moreover, it is argued that since a lamella touching a division site must form two new Plateau borders (Figure 6b) the lamella may be drained of liquid and coalesce in the process (59). Second, Prieditis (41) has shown that the likelihood of bubble division depends upon the occupancy of surrounding pores. In the absence of foam bubbles or lamella surrounding the branch point, division proceeds. However, nearby trapped foam bubbles greatly reduce the number of branch points. Stationary bubbles or lamellae divert the once branching flow down one path by acting as flexible pore walls. Division is thus prohibited.

Figure 7 illustrates the third foam generation mechanism (60). Leave-behind begins as two gas menisci invade adjacent liquid-filled pore bodies (Figure 7a). A lens is left behind as the two menisci converge downstream. As long as the capillary pressure of the medium is not too high and the pressure gradient not too large, a stationary stable lens emerges (Figure 7b). Later, the lens may drain to a thin film.

Lenses created by leave-behind are generally oriented parallel to the local direction of flow (i.e., the pore-level flow that created them) and do not make the gas phase discontinuous. If leave-behind is the only form of lens or lamella generation, a continuous-gas foam results. Ransohoff and Radke (60) found that foam generated solely by leave-behind gave approximately a five-fold reduction in steady-state gas permeability, whereas discontinuous-gas foams created by snap-off resulted in a several-hundred fold reduction in gas mobility (20,61).

We assert that snap-off is the dominant foam generation mechanism, especially under conditions of coinjection of surfactant solution and gas. The effluent bubble-size measurements from Berea sandstone of Ettinger and Radke (20), referred to earlier, show that foam coarsens with increasing gas rate. The rate of division events is greater at higher gas flow rate. Thus, if bubble generation by division were significant, foam should not be shear thinning, as is routinely observed (c.f., 20,21,61,62). In light of the significant fraction of foam which is trapped (38,39), of foam shear-thinning behavior, and of Prieditis's observations (41) noting the reduced availability of bubble division sites in the presence of stationary foam bubbles, division does not appear to be the major source of flowing lamellae in our studies with sandstones. Leave-behind is a nonrepetitive process and alone cannot account for the high flow resistances measured with foam. Finally, direct observations of foam generation in transparent etched-glass micromodels (25-27) suggest the dominance of the snap-off mechanism.

Foam Destruction

Net foam generation cannot continue unchecked. It is balanced by foam destruction processes. Chambers and Radke (26) enunciate two basic mechanisms of foam coalescence: capillary suction and gas diffusion. Because capillary-suction coalescence is the primary

mechanism for lamellae breakage, we focus on it, and only briefly touch upon foam coarsening by gas diffusion.

In stark contrast to snap-off, capillary-suction coalescence is strongly affected by surfactant formulation. Thin lamellae are not thermodynamically stable. They owe their existence to excess normal forces within the films originating from long-range intermolecular interactions. Derjaguin and coworkers (63,64) first introduced this idea in terms of a film disjoining pressure, Π , which is a function of film thickness, h . Positive values of Π reflect net repulsive film forces while negative values of Π indicate net attractive forces. Adsorption of ionic surfactant at each gas/liquid surface of the film originate the excess repulsive forces. The identically charged surfaces repel each other through overlap of their double-layer ionic clouds. At small film thicknesses protrusion and/or hydration forces give rise to a very steep repulsion. These two stabilizing forces are sensitive to surfactant concentration and structure, and ionic content of the aqueous solution. It is here that surfactant formulation comes into play for designing effective foamers. Additionally, attractive van der Waals forces tend to destabilize the film. Combination of these three forces leads to an S-shaped disjoining pressure isotherm that is similar in form to a pressure-volume isotherm for real gases and liquids. Many sources elaborate on the origin and behavior of disjoining forces in surfactant-stabilized foam films (26,55,63-71).

A recently measured disjoining pressure isotherm of an isolated lamella is shown in Figure 8 for the surfactant sodium dodecylsulfate (SDS) at 10^{-3} kmol/m³ in aqueous 0.01 kmol/m³ sodium chloride brine (65). A solid line connects the data points for three independent experimental runs, shown by various symbols. The negative, attractive portion of the isotherm between thicknesses of about 4 and 5 nm is not sketched since equilibrium measurements are not possible there. The measured isotherm indeed obeys the classic S-shape. It is well-known that film metastability demands that the slope of the isotherm be negative (26,72). For positive slopes even the slightest infinitesimal disturbance ruptures the film. Thus, the lamella in Figure 8 can exist only along the two repulsive branches near 4 nm and above 7 nm. The thicker branch or common black film arises from electrostatic overlap forces while the inner branch or Newton black film arises

from strong protrusion/hydration forces. van der Waals dispersion forces explain the middle unstable branch.

The line drawn through the disjoining pressure Π_1 reveals that three equilibrium film thicknesses are possible, roughly 4, 5, and 9 nm. Which film thickness is operative for lamellae in porous media is determined primarily by the augmented Young-Laplace equation (67-69):

$$P_c = 2\sigma C_m + \Pi(h), \quad (1)$$

where P_c is the local capillary pressure, C_m is the mean interfacial curvature of the thin film, and σ is the bulk surface tension. In the limit of thick films, the disjoining pressure approaches zero, and the classic Young-Laplace equation is recovered.

For the static, trapped lamellae, the film reaches an equilibrium thickness set by the local capillary pressure and the film curvature in obedience to Equation (1). The capillary pressure, in turn, depends on the wetting liquid saturation; the film curvature depends on the particular location within the pore structure dictated by an approximately 90° contact angle with the pore wall. As the capillary pressure in the porous medium rises during drainage, the film thickness decreases along the common black branch until Π_{\max} is reached and a Newton black film of 4 nm thickness emerges. At still higher imposed capillary pressures, a disjoining pressure is attained, Π_{rup} , not labeled on Figure 8, where the film eventually ruptures. In a foam-laden porous medium, the capillary pressure of an equivalent undispersed two-phase system corresponding to Π_{rup} is termed here the critical capillary pressure for rupture. For bulk systems Π_{rup} is a well-documented parameter controlling the stability of the foam (71). Note in Figure 8 that even a very dilute SDS surfactant solution exhibits a critical capillary pressure for rupture greater than 100 kPa (i.e., greater than 1 atm) and creates highly robust foam films. We caution that not all surfactant-stabilized foam films display an inner branch. In this case the critical capillary pressure for rupture equals Π_{\max} .

The message from Figure 8 is that static lamellae are stable to small disturbances until a critical capillary pressure is attained; then coalescence is catastrophic. In porous media it is the liquid saturation, absolute permeability, and surface tension that control this critical capillary pressure through the Leverett J-function (73). Of course, static lamellae may coalesce at lower capillary pressures if they are subjected to large disturbances. Figure 8 also reveals that static lamellae in equilibrium with the imposed capillary pressure are amazingly thin.

Coalescence behavior of flowing foam bubbles is more complicated than that of static lamellae. Khatib et al. (62) directly measured capillary pressures in 70 to 9000 μm^2 glass beadpacks during steady foam flow over a wide range of gas fractional flows from 0.1 to 0.99. For a given surfactant system they observed drastic foam coarsening at a specific capillary pressure (typically near 3 kPa), called the limiting capillary pressure, P_c^* . Above P_c^* coalescence of flowing lamellae is significant while below P_c^* it is minimal. Limiting capillary pressures for strong coalescence varied with gas flow rate and absolute permeability in addition to surfactant formulation (62).

The experimentally determined limiting capillary pressures of Khatib et al. are likely connected to the critical disjoining pressures for rupture from Figure 8. To make this connection Jiménez and Radke (55) proposed a simple hydrodynamic-stability theory which describes the thickness evolution of a lamella translating through a periodically constricted tube. Figure 9 presents one such lamella at successive times t_1 , t_2 , and t_3 . As the lamella translates from left to right, it is squeezed upon entering the constriction at time t_2 . Film thickness increases to conserve liquid mass and the disjoining pressure is correspondingly low. Jiménez and Radke assumed the ensemble-averaged curvature of the flowing thin films to be negligible compared to the capillary-suction pressure exerted by the porous medium on the Plateau border, so that the film drains to equalize P_c and Π . Drainage is driven by the pressure difference ($P_c - \Pi$). Fluid resistance in the film is inversely proportional to the local film thickness to the 3rd power, so drainage is not instantaneous.

When the lamella moves out of the pore constriction, it is stretched upon expansion into the downstream body. The film thins to conserve mass and the disjoining pressure is now high. Here the film fills in an attempt to equalize P_C and Π , again driven by the pressure difference ($P_C - \Pi$). Thus, the thickness of the transporting lamella oscillates about the equilibrium thickness established in the stationary lamellae in a sequence of squeezing/stretching, draining/filling events. Thickness oscillations are wider the higher the gas flow rate and the larger the pore-body to pore-throat aspect ratio, R_b/R_c . Jiménez and Radke (55) argue that translating lamellae break instantaneously whenever the film thickness diminishes to h_{max} , corresponding to Π_{max} in Figure 8. Thus, if the film is stretched too rapidly for healing surfactant solution to flow into the film and stabilize it, rupture ensues. The capillary pressure at which the translating lamella ruptures is defined as P_C^* , the limiting capillary pressure. The theory of Jiménez and Radke predicts that P_C^* lies below Π_{max} to an extent that increases strongly with larger pore-body to pore-throat aspect ratio and increases weakly with larger gas flow rate. For a given gas flow rate and surfactant composition, specific pore throat-pore body combinations in the medium, called termination sites (26,55), lead to capillary-suction coalescence. At low wetting phase saturation, corresponding to high capillary pressure, large numbers of termination sites are unavailed because even small aspect ratios can stretch the lamella rapidly enough to cause rupture. Simply not enough wetting phase is available to heal and stabilize the films.

The proposed model of Jiménez and Radke (55) is over-simplified in that it does not account for the details of the actual curved-film breakup (74) or for any surface tension gradients and elastic effects as the film stretches and squeezes. Nevertheless, it does correctly explain the gas-velocity dependence of P_C^* measured by Khatib et al. (62). Moreover, Huh et al. (75) studied the behavior of CO₂ aqueous surfactant foams in glass micromodels and reported visual observations of the stretching-squeezing mechanism. Lamellae coalesced in the pore bodies of the micromodel. Likewise, Chambers and Radke present photomicrographs of the identical mechanism for coalescence of N₂ aqueous surfactant foams in etched-glass micromodels (cf., Figure 26 (26)).

The basic premise underlying capillary-suction coalescence is that surfactant solutions which exhibit large rupture disjoining pressures lead to strong foam in porous media with large flow resistance. Aronson et al. (76) recently investigated this premise. They measured disjoining pressures of single foam films for SDS at several concentrations and brine levels similar to that in Figure 8; with the identical surfactant solutions they measured the steady pressure drops of N₂ foams at gas fractional flows of 90 % in 2.3 μm² glass beadpacks. Figure 10 summarizes their findings.

Open symbols in the figure correspond to the measured rupture disjoining pressures of the single aqueous SDS foam films as a function of NaCl concentration at two surfactant concentrations. Upward directed arrows on some of the experimental points indicate that the rupture pressure is larger than the value shown. Dashed lines simply sketch in the observed trends that increased surfactant and salt concentrations yield increased values of Π_{rup} . Conversely, closed symbols correspond to the measured steady pressure gradients for the same solutions. Solid lines again indicate the trends. The postulate that large rupture disjoining pressures, above 30 kPa in Figure 10, give rise to strong foam in porous media is clearly confirmed. Aronson et al. (76) estimate that the capillary pressures in their beadpacks during steady foam flow are near 1 to 5 kPa. Figure 10 then reveals that once the rupture pressure of the foam films exceed the capillary pressure of the medium, low mobility foam emerges. It is also fascinating that the low SDS concentrations of 10⁻³ M can produce very large pressure gradients. Finally, Khatib et al. (62) in their direct capillary pressure measurements also found that increased brine content increased P_C^* , consonant with the disjoining pressure measurements in Figure 10. The study of Aronson et al. (76) provides striking confirmation of the origin of limiting capillary pressures and their role in foam coalescence in porous media.

The second mechanism for foam coalescence in porous media, gas diffusion, pertains primarily to the stagnant, trapped bubbles. According to the Young-Laplace equation, gas on the concave side of a curved foam film is at a higher pressure and, hence, higher chemical potential than that on the convex side. Driven by this difference in chemical potential, gas dissolves in the

liquid film and escapes by diffusion from the concave to the convex side of the film. The rate of escape is proportional to film curvature squared and, therefore, is rapid for small bubbles (16, 26)

Bulk foams coarsen with larger bubbles growing at the expense of smaller ones that eventually disappear. However, confined foam in porous media does not coarsen in a similar fashion because bubble volume is not directly related to film curvature. Rather, in porous media lamella curvature depends on pore dimensions and on location within the pore space. Gas diffusion still proceeds from the most highly concave bubbles forcing the lamellae to diminish their curvatures by translation toward pore throats. In the absence of an imposed pressure gradient, it is possible for gas diffusion to drive all lamellae to pore throats to achieve an equilibrium state of zero curvature. Coalescence occurs only when two lamellae happen to reach the same pore throat. In the case of steam foam, coarsening is more rapid because water can condense on one side of a lamella and evaporate from the other. A noncondensable gas may be added to retard coarsening (3). Nevertheless, coarsening of the trapped foam by gas diffusion is expected. As the resulting texture diminishes, a portion of the trapped bubbles may remobilize (26).

Foam Flow at Limiting Capillary Pressure

Most foams in porous sandpacks and sandstones achieve steady flow near or at P_c^* provided the gas fractional flow is high but below unity, and provided flow rates are fixed (20, 36, 61, 62, 77-80). In the limiting capillary pressure regime the wetting liquid saturation is sensibly constant independent of gas and liquid velocities over a rather large range. This limiting saturation is thought to reflect a constant P_c^* , which, from our preceding discussion, is set primarily by the disjoining pressure isotherm of the stabilizing surfactant.

Foam flow behavior in the limiting capillary regime is rather remarkable (20, 36, 61, 62, 79-81). When liquid velocity is held constant and gas velocity is adjusted, pressure drop is independent of gas flow rate. Varying liquid velocity and holding gas velocity constant usually yields a linearly increasing pressure drop response. Increasing both liquid and gas velocity while

holding the fractional flow constant yields a linear response when pressure drop is plotted versus total flow rate. Finally, steady-state saturations are independent of gas fractional flow. These observations can not be explained by Darcy's law for multiphase flow in porous media. In particular, foam flow is not solely a function of fractional flow, but depends on individual gas and liquid velocities.

The consequences of foam flow in the limiting capillary pressure regime are important. Khatib et al. (62) point out that whenever P_C^* is achieved in a porous medium, relative gas mobility is easily calculated. Because P_C is constant, aqueous-phase saturation consequently remains constant and so does the relative permeability to the wetting liquid (c.f., discussion of Figure 4). Since pressure gradients in both the wetting and nonwetting phases (foam) are identical at steady state, Darcy's law for the aqueous phase determines foam-flow behavior. Persoff et al. (61) expand this point and demonstrate experimentally that within the limiting capillary pressure regime, only one or two measurements of foam pressure drop are needed to predict the entire spectrum of steady-state results. Rossen (30, 82), by incorporating the above observations into fractional flow theory, demonstrates how powerful the limiting capillary regime is in understanding foam flow.

Not all foam flow behavior falls in the limiting capillary pressure regime, even for constant-rate injection at steady state. Deviations are evident at low gas fractional flow (i.e., low quality foam). In a $1.3 \mu\text{m}^2$ Boise sandstone, nitrogen gas fractional flows spanning from 0.7 to 0.995 were found to be within the limiting capillary pressure regime (61). In fact, Persoff et al. (61) could not find a lower limit to the regime. Likewise, Ettinger and Radke (20) probed fractional flows between 0.7 and 0.9 finding no lower limit to limiting capillary-pressure behavior. However, the data of Khatib et al. (62) for 70 to 9000 μm^2 beadpacks and those of De Vries and Wit (36) for sandpacks ($4.2 \mu\text{m}^2$) and a Bentheim sandstone ($1.2 \mu\text{m}^2$) show that at lower gas fractional flows pressure drop increases as gas flow rate is increased at a fixed liquid flow rate. This behavior continues up until a break point or maximum gas fractional flow where the limiting capillary pressure is reached. Above fractional flows of roughly 0.92, pressure drop for fixed

liquid flow rates is essentially independent of gas flow rate indicative of the limiting capillary pressure regime.

More recently, Osterloh and Jante (77) probed a wide range of flow rates and fractional flows for foam in a $6.2 \mu\text{m}^2$ sandpack. They distinguish two regimes. At gas fractional flows above 0.94, the pressure gradient was reasonably independent of gas velocity (at fixed liquid velocity) but varied with liquid velocity (at constant gas velocity) to roughly the 1/3 power. Also, liquid saturation was nearly constant at 6%. At lesser gas fractional flows the converse was found. Pressure-gradient response was negligible with increased liquid velocity but increased with gas velocity to the 0.31 power. They surmised that the transition between the two regimes occurs at the point where the limiting capillary pressure is attained.

The variation in the range of fractional flows yielding limiting capillary pressure behavior is likely due to the different surfactant systems employed. Different surfactant structures and conditions such as concentration and temperature lead to different disjoining pressure isotherms for single foam films and thus different limiting-capillary-pressure characteristics. Also, the various porous media have differing capillary pressure versus aqueous phase saturation relationships. Although the limiting capillary pressure regime is by no means general for all conditions of foam flow in porous media, it is an important one. Our modeling effort to follow is directed toward predicting how this behavior emerges in a transient, one-dimensional foam displacement.

Population-Balance Modeling of Foam Flow in Porous Media

A variety of methods have been proposed for modeling of foam flow and displacement in porous media. These range from population-balance methods (8,9,20,39,78-80,83) to percolation models (42-45,47,84) and from semi-empirical alteration of gas-phase mobilities (85-92) to applying so-called fractional flow theories (30,82). Semi-empirical models are computationally simple, but they lack generality. The last method may be unsuitable for modeling of foam flooding because fractional flow theory is approximate when applied to compressible phases (30), severe

extrapolations from available data are needed to fit model parameters (30), and strong foam behavior is not in general a unique function of fractional flow (c.f., 20,36,61,62,75,81). Constructing fractional flow curves for foam flow in porous media, as such, may be inappropriate as absolute flow rates determine foam flow behavior.

Of these four methods, only the population-balance method and network or percolation models arise from first principles. Network models, while allowing replication of pore-level mechanisms, have the decided disadvantage of requiring large amounts of computation time and provide results on a prohibitively small grid. It seems unlikely that either network or percolation models can be useful in transient displacements that demand tracking of saturation, surfactant concentration, and foam on laboratory scale let alone field scales.

The population-balance method for modeling foam flow (8,9) was originally proposed because it incorporates foam into reservoir simulators in a manner that is identical to calculating the transport of mass and energy in porous media. Further, the method is mechanistic in that it can account for the actual pore-level events described in the previous sections. In its minimal form, the population balance simply adds another component to a standard multicomponent simulator. By analogy to balances on surfactant or other chemical species, a separate conservation equation is written for the concentration of foam bubbles. Our goal, in this section, is to map out a population balance that is easy to implement, fits simply into the framework of current reservoir simulators, and employs a minimum of physically meaningful parameters descriptive of the dominant pore-level events. We focus on transient displacement by strong foam that at steady state achieves the limiting capillary pressure regime.

Conservation Equations

The mass balance equations for the gaseous and aqueous phases are written in standard reservoir simulator form (c.f., 10,93). For the nonwetting foam or gas phase in a one-dimensional medium we write

$$\frac{\partial[\phi\rho_g S_g]}{\partial t} + \frac{\partial(\rho_g u_g)}{\partial x} = q_g \quad (2)$$

where t denotes time and x gives the axial location. ϕ is the porosity of the porous medium, ρ_g is the gas mass density, S_g is the saturation of the gas phase, u_g the superficial or Darcy velocity, and q_g is a source/sink term for gas used here to apply boundary conditions (10). The companion mass balance for the aqueous phase is written by interchanging the subscript g denoting gas for w denoting the liquid phase.

A mass balance on surfactant is also required, which written in standard form becomes

$$\frac{\partial[\phi(C_s S_w + \Gamma)]}{\partial t} + \frac{\partial(u_w C_s)}{\partial x} = Q_s \quad , \quad (3)$$

where C_s is the number or molar concentration of surfactant in the aqueous phase, Γ is the amount of surfactant adsorption on the rock surfaces in units of moles per void volume, and Q_s is the source/sink term for surfactant in units of moles/volume/time.

Since the mobility of the foam phase is a strong function of texture (9,18,20,26,33,48), mechanistic prediction of foam flow in porous media is impossible without a conservation statement accounting for the evolution of foam bubble size (8). Following Patzek (8) and others (9,39) we write a transient population balance on the mean bubble size:

$$\frac{\partial[\phi(S_f n_f + S_t n_t)]}{\partial t} + \frac{\partial(u_f n_f)}{\partial x} = \phi S_g (r_g - r_c) + Q_b \quad . \quad (4)$$

In Equation (4), the subscripts f and t refer to flowing and trapped foam, respectively, and n_i is the foam texture or bubble number density. Thus, n_f and n_t are, respectively, the number of foam bubbles per unit volume of flowing and stationary gas. The total gas saturation is given by $S_g = 1 - S_w = S_f + S_t$, and Q_b is a source/sink term for foam bubbles in units of number per unit volume per unit time. The first term of the time derivative is the rate at which flowing foam texture becomes finer or coarser per unit rock volume while the second is the net rate at which foam

bubbles trap. The spatial term tracks the convection of foam bubbles. The usefulness of a foam-bubble population balance, in large part, revolves around the convection of gas and aqueous phases.

On the right of Equation (4), we express generation and coalescence rates, r_g and r_c , on a per volume of gas basis. These two terms are fundamental for they control bubble texture. At steady state, far from any sources or sinks, and where rock properties are constant (e.g., absolute permeability, relative permeability, and capillary pressure functions), bubble size is set by $r_g = r_c$. That is, the rate of bubble generation by snap-off balances the rate of bubble coalescence by capillary pressure suction (20). To proceed, kinetic expressions are needed for r_g and r_c .

Generation

Snap-off in germination sites determines the rate expression for bubble generation following the process pictured in Figure 5. We neglect bubble leave-behind. The division mechanism for producing new lamella yields a rate that is indistinguishable in form from that of coalescence and is included there. Earlier studies (9,39,94) argue that the frequency of snap-off events is inversely proportional to the sum of the time to displace a newly formed lens out of the constriction and the time for wetting liquid to drain back along the pore corners to initiate pinch-off of another lens. The proportionality constant counts the number of active germination sites. By extending the hydrodynamic analysis of Ransohoff et al. (94) for constricted, cornered pores to include imposed wetting liquid flow, Kovscek (80) finds that snap-off frequency may be expressed as linearly proportional to liquid velocity and to gas velocity raised to a power less than unity. The liquid-velocity dependence originates from the net imposed liquid flow, while the gas-velocity dependence arises from the time for the lens to exit the pore. Accordingly, we write that

$$r_g = k_1 v_f^a v_w^b \quad , \quad (5)$$

where $v_w = u_w / \phi S_w$ is the local interstitial liquid velocity, and $v_f = u_f / \phi S_f$ is the local interstitial velocity of the flowing foam. These velocities depend upon the local saturation of flowing liquid or gas and the local pressure gradient which can include capillary pressure and gravitational effects; a and b are power indices, with the index b close to unity. Equation (5) suggests that bubbles are produced only in the portion of the foam that transports. The generation rate constant, k_1 , reflects the number of foam germination sites. Intuitively, as liquid saturation falls the number of germination sites falls. We take k_1 as a constant here. Of course, the bubble generation rate does vary implicitly with liquid saturation through the dependencies on liquid and gas velocities. No surfactant properties appear in Equation (5) consistent with the mechanical origin of snap-off.

Falls et al. (9) and Friedmann et al. (39) point out that if a lamella arrives at a germination site prior to the total elapsed time for snap-off, then snap-off is precluded. An upper limit is then placed on the evolution of foam texture. We find in our systems that strong coalescence forces come into play before this upper limit is attained.

Some researchers have found a so-called critical velocity for the onset of foam generation (39,45,60). Friedmann et al. (39) generate foam in sandstone cores at different, initial, surfactant-laden water saturations after steady gas and surfactant-free liquid flow is established. Critical onset velocities increase with decreasing S_w . Velocities up to several hundred meters per day are reported when the initial water saturation is low. Once steady two-phase flow is established, high gas velocities are apparently required for the gas to build a sufficient pressure gradient and enter into wetting liquid-filled pores (e.g., as in Figure 5).

The existence of a critical velocity for the appearance of strong foam is linked, apparently, to the initial condition of the porous medium. Recent experiments in glass beadpacks, and in Boise and Berea sandstones have not confirmed that a critical gas velocity or pressure drop must be exceeded for successful foam generation (21,61,78,95,96). In all of these cases the porous media were completely saturated with surfactant solution prior to any gas injection. With initial high water saturations foam readily generates. In the experiments and modeling calculations to follow, the

initial water saturation is 100 %. For this reason we do not include a critical onset velocity or pressure gradient in Equation (5).

Coalescence

A pore-level based rate expression for capillary-suction coalescence is readily obtained. Figure 9 illustrates that foam lamellae are destroyed in proportion to their flux (i.e., $v_f n_f$) into termination sites. Hence, we write that (20)

$$r_c = k_{-1}(S_w) v_f n_f, \quad (6)$$

where $k_{-1}(S_w)$ is a coalescence rate constant that varies strongly with local aqueous-phase saturation, S_w , and n_f is again the number of bubbles per unit volume of the flowing foam. Additionally, the coalescence rate constant also varies with surfactant concentration and formulation. Equation (6) teaches that higher interstitial gas velocities lead to increased foam coalescence because rapidly stretched lamellae are more vulnerable to breakage. Per our earlier discussion, sufficient time does not exist for surfactant solution to flow into a rapidly stretched lamella and heal it.

As coalescence depends upon P_c^* , the coalescence rate constant depends strongly upon surfactant formulation, concentration, and S_w . Weak surfactants and/or low concentrations make $k_{-1}(S_w)$ quite large. Additionally, the saturation dependence of $k_{-1}(S_w)$ is quite dramatic. Khatib et al. (62) have shown that for strongly foaming solutions $k_{-1}(S_w)$ is small for high aqueous phase saturations but rises steeply as S_w falls to a value corresponding to the limiting capillary pressure. If the aqueous phase saturation falls near or below that corresponding to the limiting capillary pressure $k_{-1}(S_w)$ approaches infinity. Cognizant of these observations, we write that

$$k_{-1}(S_w) = k_{-1}^o \frac{(1 - S_w)}{(S_w - S_w^*)} \quad (7)$$

where S_w^* is the saturation corresponding to the limiting capillary pressure. Equation (7) allows the coalescence rate to increase monotonically as the porous medium desaturates. As desired, the coalescence rate becomes infinite at S_w^* . It is important to emphasize that the sensitivity of foam to surfactant formulation is embodied in S_w^* . Foamers with high critical rupture disjoining pressures result in high limiting capillary pressures, P_c^* . The capillary pressure curve for the particular medium then sets a low value of S_w^* and, accordingly, a low foam mobility.

Figure 11 displays qualitatively the dependence of both coalescence and generation rates on the wetting liquid saturation. Note that S_w^* , the aqueous saturation corresponding to the limiting capillary pressure, is not the same as the traditional connate water saturation and may be either smaller or larger than S_{wc} depending on the surfactant formulation and the nature of the porous medium. Near S_w^* the rate of foam coalescence rises steeply as P_c in the medium approaches Π_{rup} . The intersection of the two rate curves determines the relationship between the steady state liquid saturation and foam texture from Equations (5) through (7). Because of the steepness of the coalescence rate with S_w , changes in gas or liquid velocity have little effect on the steady saturation. This explains the lack of sensitivity of the wetting liquid saturation to flow rates seen in the limiting capillary pressure foam flow regime (20,36,61,62,77,78).

It is readily argued that the intersection of coalescence and generation rates in Figure 11 leads to a stable steady state. If the system is perturbed away from this point, it naturally returns. Consider a small, positive perturbation in the local liquid saturation. The coalescence rate then declines and the foam texture becomes finer. This causes an increased flow resistance, which then returns the liquid saturation back to the stable operating point. The converse negative saturation perturbation is similarly argued to be stable.

The rate of bubble division, the second mechanism for creating foam, is proportional to the flux of lamellae into division sites (20). Thus, the rate of foam generation by division is formally identical to Equation (6). Further, both rate constants share the property of being small when S_w is high, since more division sites become available as S_w drops. It is thus difficult to distinguish between division and coalescence when writing mechanistic rate expressions. We do not do so

here. Additionally, equating capillary-suction coalescence and bubble-division generation rates teaches that, if division is the primary foam generation mechanism, foam texture at steady state is independent of gas rate. From our discussion on foam microstructure, this is not the experimental result (20,21, 62). Finally, as gas diffusion coarsening of the trapped phase is not currently well understood, we do not include it in our simulations.

Gas Mobility

In addition to bubble kinetic expressions the mass balance statements in Equations (2) through (4) demand flow-rate relationships for the foam and wetting liquid phases. From our discussion of Figures 2 through 4 the confined foam is divided into intermediate wetting trapped and nonwetting flowing portions. For the flowing foam the structure of Darcy's law is retained:

$$u_f = \frac{K k_{rf}}{\mu_f} \left(-\frac{\partial p_g}{\partial x} \right) \quad (8)$$

where K is the absolute permeability, k_{rf} is the relative permeability to the flowing foam, and μ_f is the foam effective viscosity. Equation (8) does not imply Darcy flow because μ_f is not a constant. Based on the theoretical studies of Bretherton (51) and Hirasaki and Lawson (18), we adopt the following expression for the non-Newtonian foam effective viscosity:

$$\mu_f = \mu_g + \frac{\alpha n_f}{v_f^c}, \quad (9)$$

where α is a constant of proportionality dependent primarily on the surfactant system. Others have written similar expressions (20,39,48). According to Equation (9), foam viscosity increases with finer textured foams but decreases with increasing interstitial velocity. In the absence of flowing foam bubbles (i.e., $n_f = 0$) the gas viscosity of a continuous foam is recovered. Friedmann et al. (39) report an empirical value of 0.29 for the exponent c . The Bretherton-based theoretical value is 1/3 (18,48,51,97).

Again, since the portion of foam that actually flows partitions into the largest and, hence, least resistive channels while the trapped fraction partitions into the intermediate-sized pores, and wetting liquid flows in the smallest most resistive channels (cf., Figure 4), a Stone-type model (53) for relative permeability is appropriate. That is, the relative permeability of the most nonwetting phase (i.e., flowing foam) is a function of the saturation of the most nonwetting phase. In accordance with (53), we write that

$$k_{rf} = k_{rg}^o S_{fd}^g \quad (10a)$$

where

$$S_{fd} = X_f (1 - S_{wd}) \quad (10b)$$

and

$$S_{wd} = \frac{(S_w - S_{wc})}{(1 - S_{wc})} \quad (10c)$$

$X_f = S_f/S_g$ is the fraction of the foam phase that is flowing. Flowing foam relative permeability is a function of the saturation of flowing gas and, consequently, is greatly reduced compared to the case of a free gas propagating through the porous medium at the total gas saturation. Standard Corey exponent models are adopted for the relative permeability functions with g representing the exponent for gas flow (98). The subscript d indicates that the aqueous-phase saturation is normalized over the saturation range where two-phase flow occurs, and S_{wc} is the connate aqueous phase saturation. k_{rf} ($=k_{rg}$) is obtained from relative-permeability measurements for continuum gas-liquid flow in the porous medium.

Consonant with Figure 4, Stone's model for relative permeability also implies that the relative permeability for the aqueous wetting phase is unaffected by the presence of foam. Hence, Darcy's law in Equation (8) is written for the wetting liquid with

$$k_{rw} = k_{rw}^o S_{wd}^f \quad , \quad (11)$$

where f is the Corey exponent for liquid flow. Recall that this framework confirms the experimental result that during foam flow the aqueous phase distributes into its own separate wetting channels (15,33-36). Again, $k_{rw}(S_w)$ is known from studies on continuum two-phase flow in the medium.

Clearly, the relative permeability of the trapped foam is zero. However, knowledge of the fraction of foam trapped in the porous medium is needed to complete the flow model. In general, the fraction of foam trapped, $X_t = S_t/S_g$, is a function of pressure gradient, capillary pressure, aqueous-phase saturation, and pore geometry. So far, the trapped gas fraction has only been measured for experimental systems at steady state (38,39). Percolation models, on the other hand, hold promise for determining the functional dependence of X_t (42-47). We write the trapped fraction as a function of the trapped texture, n_t :

$$X_t = X_{t,max} \left(\frac{\beta n_t}{1 + \beta n_t} \right) \quad , \quad (12)$$

where $X_{t,max}$ is the maximum fraction of trapped foam, and β is a trapping parameter. Equation (12) demands no trapping when the trapped texture is zero and a smooth rise to a maximum trapping for finer textured bubbles. The trapped fraction, $X_t = 1 - X_f$, strongly influences the foam flow resistance by reducing gas-phase relative permeability through Equation (10b).

To relate the flowing and trapped textures we follow Friedmann et al. (39) and assume local equilibrium. We argue that during coinjection of gas and liquid the trapped fraction is

dynamic. Some portion of the trapped bubbles coarsen and remobilize to be replaced by subsequent trapping of flowing bubbles. Flowing and stationary texture are thus approximately the same. In the simulations to follow we set n_f equal to n_t .

To complete the model phase-equilibria information is required. The aqueous surfactant phase is assumed incompressible and nonvolatile; the gas (i.e., N_2) in the foam phase is insoluble and obeys the ideal gas law. In our experiments surfactant is present in equal concentration throughout the aqueous phase and rock adsorption is satisfied. Thus, the surfactant balance in Equation (3) is automatically satisfied.

In principle, our framework of separating foam mobility into effective viscosity and relative permeability components also permits description of continuous foam. If only free gas flows, then n_f is zero, and the bulk gas viscosity emerges naturally from Equation (9). It is, however, no longer possible to couple the flowing and trapped textures. An independent theory for X_t is required.

Making and Breaking

Individual bubbles in the foam phase do not retain their identities over macroscopic distances. Rather, they coalesce and reform by the pore-level making and breaking processes outlined earlier. Some authors ([75,84,99](#)), however, use the phrase "making and breaking" in a strict sense attributed originally to Holm ([15](#)). After a lamella is produced at a pore constriction, it translates only a short distance not exceeding the exit pore body before it ruptures. The process then repeats so that on the average the pore is blocked for a fraction of time depending on the stability of the lamellae. Careful reading of Holm's discussion, however, reveals that no such specific meaning is attached to the term "making and breaking". To avoid possible misinterpretation we refrain from using this phrase altogether.

Nevertheless, it is important to point out that a lamella cannot be created directly at a pore throat. Rather, a lens forms first with lamella creation occurring upon expansion into the adjacent pore body, provided surfactant is available (cf., the discussion of foam-generation mechanisms). During two-phase flow without stabilizing surfactant present, lenses are still created by snap-off in

Roof sites (54, 60) followed by expansion and rapid coalescence in the downstream pore body, once the lens thins to a film. If stabilized lamellae are pictured to rupture before exiting the immediate downstream pore body, they are not much longer lived than unstable lenses. Such processes are accounted for in measurements of continuum relative permeabilities.

Experiment

The centerpiece of the apparatus is a vertically mounted, 60 cm long, 5.1 cm diameter, 1.3 μm^2 Boise sandstone core with a porosity of 0.25 mounted in a stainless steel sleeve. Nitrogen gas and foamer solution are injected at the top of the apparatus. Experiments are conducted at back pressures in excess of 5 MPa (700 psia) and at ambient temperature. In-situ saturation measurements are provided by gamma-ray densitometry. A translating carriage holding the radioactive source and detector allows sampling of saturations along the entire length of the core. Pressure taps are also located at 10 cm intervals along the core. Considerable experimental details are available elsewhere (61,78,80).

Two modifications were made to the apparatus to allow exploration of lower flow rates: gas injection is now controlled by a Brooks 5850C 100 SCCM (standard cubic centimeters per minute) mass flow controller (Emerson Electric, Hatfield, PA) and liquid injection is controlled by an ISCO 500 D syringe pump (Instrumentation Specialties Company, Lincoln, NE). Gas superficial velocities now span 0.30 to 2.13 m/day (1 to 7 ft/day) at 5MPa (700 psia) backpressure while liquid velocities as low as 9 mm/day (0.03 ft/day) are possible.

The foamer solution is a saline solution containing 0.83 wt% NaCl (J. T. Baker, reagent grade) with 0.83 wt% active C₁₄₋₁₆ α -olefin sulfonate surfactant (Bioterg AS-40, Stepan). Water is provided by a Barnstead Fi Stream II glass still (Barnstead Thermolyne Corp. Dubuque, IA). The solution surface tension is 33 mN/m measured by the Wilhelmy plate method, and the solution viscosity is 1 mPa·s. Bottled nitrogen is the gas source.

The core is initially completely saturated with aqueous foamer solution with rock adsorption satisfied. Nitrogen and aqueous surfactant solution are then injected at fixed flow rates until steady state is achieved. Transient pressure and aqueous saturation profiles are monitored for a wide range of gas and liquid flows. Only one transient foam displacement is reported here. Additional results are available elsewhere (78-80).

Comparison of Theory and Experiment

To model the measured transient foam displacements, Equations (2) through (12) are rewritten in standard implicit-pressure, explicit-saturation (IMPES) finite difference form with upstream weighting of the phase mobilities following standard reservoir simulation practice (10). Iteration of the nonlinear algebraic equations is by Newton's method. The three primitive unknowns are pressure, gas-phase saturation, and bubble density. Four boundary conditions are necessary, since the differential mass balances are second order in pressure and first order in saturation and bubble concentration. We fix the outlet pressure and the inlet superficial velocities of gas and liquid. No foam is injected so Q_b is set to zero in Equation (4). Initial conditions include $S_w = 1$, $n_f = 0$, $C_s = 0.83$ wt%, and a fixed (back) pressure. Calculations require less than 1 cpu minute on a VAX 6420 computer. The thesis of Kovsky provides additional numerical details (80).

Model Parameters

Table 1 lists the model parameters, eighteen in all. Those applicable to standard, two-phase flow are shown to the left. They include the absolute rock permeability and porosity, phase viscosities, and Corey exponents and scaling constants for the continuum relative permeabilities. Information on the Boise core, including the relative permeabilities of nitrogen and water, is available from the experiments of Persoff et al. (61). We fit Equations (10) and (11) to those independently measured relative permeabilities.

Nine additional parameters are demanded to predict foam displacement, as listed to the right of Table 1. They include the generation and coalescence rate constants, the exponents a and b for the generation rate expression, the saturation, S_w^* , corresponding to the limiting capillary pressure, the proportionality constant and velocity exponent for the foam effective viscosity, and the parameters for the trapped foam fraction. All have clear physical meaning. Thus, the exponent for the effective viscosity, c in Equation (9) is set to $1/3$ following extensions of the Bretherton analysis (18,97). Also the theoretical calculations of Roof snap-off behavior in constricted, cornered pores by Kovscek (80) teach that $b = 1$ and that a is less than unity.

All but one of the remaining population-balance parameters are determined from steady-state behavior of foam flow. Fortunately, this exercise drastically limits the choice of parameter values. Thus, for our strong foamer solution we choose $S_w^* = 0.26$, which is slightly above connate saturation (20,61,78), and $X_{t,max} = 0.9$ based on the experimental tracer studies of trapped gas saturations (38,39).

Next, the exponent a is needed to specify the gas-velocity dependence of foam generation in Equation (5). As pointed out earlier, in the limiting capillary pressure regime with strong foamers the steady foam flow pressure drop is sensibly independent of gas flow and varies linearly with liquid velocity (20,36,61,80). When $r_g - r_c = 0$, Equations (5) and (6) along with the foam flow rheology predicted by Equations (8) and (9) reveal that $a = 1/3$, confirming the restriction of $a < 1$. The theoretical value of $b = 1$ demands a linear dependence of steady foam pressure drop on liquid velocity. The choices of $a = c = 1/3$ and $b = 1$ predict that foam texture must coarsen at higher gas velocity. This result, though not immediately obvious, is confirmed by experiment (20). We discover here the origin of the unique flow behavior of foam in porous media as due to texture alteration with changing gas and liquid velocities, in addition to shear-thinning rheology. It is because of these changing textures that classical fractional flow theory does not apply to foam.

The important ratio, k_1/k^0_{-1} , sets the general magnitude of the bubble density. We choose steady-state textures on the order of 100 mm^{-3} or an equivalent undistorted bubble radius of about $130 \text{ }\mu\text{m}$, in agreement with the measurements of Ettinger and Radke (20). Equations (8) and (9)

combined with steady state texture now set the magnitude of the steady pressure drop and, consequently, α . It remains to specify the individual magnitudes of k_1 and k_0^{-1} . These are adjusted to confine the region of net texture refinement close to the inlet face of the porous medium (20). Thus, of the nine population-balance parameters, eight are preset by results of steady-state measurements. Finally, our simulations prove somewhat insensitive to the trapping parameter β , which is chosen such that $X_t = (1 - X_f)$ is 85% when n_f is 20 mm^{-3} .

Transient Displacement

Experimental displacement results for the simultaneous injection of aqueous surfactant solution and nitrogen into a core initially saturated with a surfactant solution are shown in Figures 12 and 13. Darcy velocities relative to the exit pressure of 4.8 MPa are 0.43 m/day (1.4 ft/day) for gas and 0.046 m/day (0.15 ft/day) for liquid yielding a gas fractional flow or foam quality of 90%. Figure 12 provides the transient liquid saturation profiles. Experimental data points are connected by dashed lines. Time is expressed nondimensionally in pore volumes, PV, which is the ratio of total volumetric flow rate (at exit pressure) multiplied by elapsed time and divided by the void volume of the core.

Experimentally, steep fronts are seen in Figure 12 whereby the aqueous saturation upstream of the front is approximately 30%, about 5 saturation units above connate saturation, and downstream it is 100%. From the saturation profiles it appears that foam moves through the rock in a piston-like displacement when saturated with surfactant solution. After the front has passed a particular location, saturation changes very little. Foam clearly provides a very efficient displacement of the aqueous phase. Figure 12 indicates that even though nitrogen and surfactant solution are injected separately, rapid foam generation and liquid desaturation occur near the inlet. Gas breakthrough is at roughly 0.80 PV and by 1.5 PV the saturation profile ceases to change. In general, we find that aqueous desaturation is complete in about 1 to 2 PV for all cases. The experimental transient data always follow the general forms shown in Figures 12 and 13 when the core is presaturated with surfactant solution (78-80).

The theoretical saturation profiles, shown as solid lines in Figure 12, track the experimental results well. Because the dissipative action of capillary pressure gradients is not included in the model formulation, calculated fronts remain steep and sharp. The population-balance model predicts that S_w is high at the core inlet. Aqueous saturation is around 76% at x/L equal to zero, but drops rapidly to approximately 30% by x/L equal to 0.2. Since no foam is injected, n_f is zero at the inlet, and the foam effective viscosity is equal to the gas viscosity. Consequently, S_w is high. Foam texture, however, rapidly increases producing a low foam mobility. Unfortunately, due to saturation scanning limitations, little experimental data are available directly at the inlet to verify the model predictions. Minssieux (100) did detect such a region of high S_w near the inlet of a sandpack during foam displacement.

A region of net foam generation near the core inlet is also witnessed in the transient pressure profiles of Figure 13. Both the experimental data (dashed lines) and model calculations (solid lines) show that pressure gradients near the inlet are definitely shallow indicating that flow resistance there is small. Steep gradients are found closely downstream of the inlet region. Again, we argue that that foam texture is coarse near the inlet.

Figure 14 reports the calculated transient foam bubble density, n_f , as a function of dimensionless distance. At all time levels, foam bubbles are coarsely textured near the inlet, but within the first fifth of the core, texture becomes much finer. Beyond the first fifth of the core, the limiting capillary pressure regime develops; foam texture in this region is nearly constant as is the liquid saturation in Figure 12. Foam texture also increases rapidly with respect to time. At 0.23 PV, foam bubble density immediately upstream of the front (i.e., $x/L = 0.35$) is within 80% of its steady state value. Figure 14 confirms that foam moves through the column in a piston-like fashion consistent with the experimental data in Figures 12 and 13. Unfortunately, no experimental method currently exists to measure bubble density in-situ.

Figures 12 through 14 further demonstrate that both model and experimental transient saturation profiles of Figure 12 are exactly tracked by the pressure and foam texture profiles of Figures 13 and 14. High pressure gradients and fine foam textures are seen where liquid saturation

is low and vice versa. Careful examination of Figures 12 through 14 points out a deficiency of the model calculations. Predicted saturation and pressure profiles build too quickly. Theoretical steady-state pressure drop and liquid saturation agree well with experiment. Transient pressures, however, are overpredicted in some regions by roughly 100 kPa (15 psi), and the foam front slightly leads the experimental one. These discrepancies are likely a result of the imposition of instantaneous equilibrium between flowing and trapped bubbles, which at early time may overpredict the amount of bubble trapping. It is also possible that the generation rate constant is reduced somewhat at high S_w (26). Nevertheless, good agreement is found between experiments for transient foam displacement and the proposed population-balance model (78-80).

Steady Behavior

New steady-state experimental (closed symbols) and model results (solid lines) are compared in Figures 15 and 16. Here we give overall pressure gradients (i.e., the ratio of pressure drop to length) rather than core pressure drops. Figure 15 portrays pressure-gradient behavior when gas injection velocity is held constant while varying liquid flow rate, whereas Figure 16 shows the results from holding liquid injection rate constant but varying gas flow rates. In Figure 15, the pressure gradient increases linearly from roughly 0.4 to 4.5 MPa/m as liquid velocity is varied between 0.012 and 0.076 m/day (0.04 and 0.25 ft/day). Except for the slight depression of the single experimental datum at roughly 0.028 m/day, the experimental points all fall on the theoretical curve within experimental error. For comparison, the pressure drop of water flowing at 0.46 m/day in $1.3 \mu\text{m}^2$ Boise sandstone is 4.1 kPa/m (0.2 psi/ft). Foam reduces gas mobility by factors approaching 5000!

Figure 16 illustrates the independence of steady foam pressure gradient to gas velocity. Model prediction of pressure drop, 1.7 MPa/m (77 psi/ft), is slightly greater than the experimental result, 1.5 MPa/m (68 psi/ft). This discrepancy is understood by comparing the constant liquid velocity (0.028 m/day) used in Figure 16 to the results in Figure 15. The only experimental data point which did not fall on the model-predicted line lies at 0.028 m/day. The data taken during that particular experiment appear to have slightly depressed pressure drops.

The steady-state pressure drop versus phase velocity trends in Figures 15 and 16 strikingly reconfirm the earlier findings of Ettinger and Radke (20) and Persoff et al. (61) obtained with differing surfactants and differing sandstone cores. The data are characteristic of the limiting capillary pressure regime, since measured steady-state liquid saturations in Figures 15 and 16 are constant near 0.3 (80). Adjustment of foam texture with changing flow rates explains the unusual behavior seen. When gas velocity increases under constant liquid flow rate conditions, foam texture coarsens, viscosity decreases, and constant pressure drop is maintained. Conversely, when liquid velocity increases while gas rates are held constant, foam texture and viscosity increase to yield a linearly rising pressure drop. Foam texture adjusts in obedience to generation and coalescence rate laws, compatible with a limiting capillary pressure and a sensibly constant and low aqueous-phase saturation at steady state. Without accounting for bubble texture such results are difficult to rationalize.

Summary

Foam flow in porous media is a complex, multifaceted process. Macroscopic results are the ensemble average of many pore-scale events that lead to bubble evolution and pore-wall interaction during multiphase flow. Foam in porous media is best understood when the undergirding pore-level phenomena are elucidated and quantified.

A porous medium shapes foam to its own liking as confined, pore-filling bubbles and lamellae. Foam in porous media is not a continuum fluid. The three mechanisms of foam generation (snap-off, division, leave-behind) are all pore geometry specific. Snap-off is a mechanical process that occurs in multiphase flow without surfactant. For successful gas-bubble snap-off, the pore body to throat constriction ratio must be sufficiently large (roughly 2) and gently sloped. Otherwise stable wetting collars form in pore throats obviating foam generation (26,54). Sufficient liquid supply must also be available for fluid accumulation in pore throats prior to pinch-off. Lamellae are never generated directly. Rather, snap-off creates a lens of aqueous fluid that later

drains later under the action of capillary suction. Division proceeds by subdividing previously generated moving foam bubbles or lamellae at points where flow branches. Thus, division requires the porous medium to be relatively free of stationary lamellae or foam bubbles that greatly reduce the number of branch points. Leave-behind generates stationary aqueous lenses while aqueous-phase saturation is high. It is a nonrepetitive process that alone cannot account for the large reduction in gas mobility seen with foam.

Foam generation does not continue unchecked. Surfactant stabilized lamellae are only metastable. Coalescence ensues when a translating lamella moves out of a sharply constricted pore throat into a body and the lamella is stretched too rapidly for healing flow of foamer solution. Whereas foam generation by capillary snap-off is independent of surfactant formulation, coalescence of foam lamellae strongly depends on surfactant formulation, concentration, and salinity.

Coalescence of flowing foam is complicated. Yet coalescence in porous media does correlate directly with rupture of single, static lamellae. If an isolated foam film can withstand large capillary suction pressures, that particular foamer solution produces a strong foam in porous media. Thus, films that exhibit large rupture disjoining pressures lead to foams with large flow resistance in porous media. A large disjoining pressure for rupture also explains the limiting capillary pressure flow regime and its sensitivity to surfactant formulation.

The mobility of gas dispersed as strong foam in porous media is low, many orders of magnitude smaller than that of the parent gas phase. Only a small percentage of the overall foam gas saturation actually flows, typically 1 to 15 percent at steady state. The stationary portion blocks intermediate-sized flow paths and lowers the effective permeability of the rock to gas. Of the remaining portion of foam that actually flows in the largest pore channels, interactions of foam bubbles with pore walls determines an effective viscosity that is larger than that for water filling the same channels. Detailed analyses of bubble flow in constricted capillaries with noncircular cross section show quite universally that foam is shear-thinning and texture dependent.

To predict foam behavior mechanistically and quantitatively it is necessary to account for bubble-size evolution. A foam-bubble population balance provides the necessary framework by including foam as a simple component in a standard reservoir simulator. Reduced gas mobility is modeled by a lowered gas relative permeability and a raised effective viscosity. A Stone-type model for relative permeability provides the requisite rules for modeling the relative permeability of both wetting liquid and nonwetting foam. Theory applied to the snap-off generation and capillary suction coalescence pore-level events, garners the specific forms of the generation and coalescence rate expressions.

Only the case of steady coinjection of surfactant solution and gas into a one-dimensional core initially filled with surfactant solution is addressed. Calculated transient foam displacement well represents both the measured wetting liquid saturations and pressure profiles with physically meaningful parameter values. It is predicted and experimentally verified that foam moves in a piston-like fashion through a linear porous medium presaturated with surfactant solution. Moreover, the proposed population balance predicts the entire spectrum of unique steady foam flow behavior in the capillary pressure regime.

The population balance is a powerful tool for modeling foam displacement and flow in porous media, since it correctly predicts the evolution of foam microstructure from well documented pore-level events and since it merges with current reservoir simulation practice. Perhaps the main power of the population-balance approach is its general framework. As understanding of mechanistic detail improves, this information may be incorporated in the modeling effort.

Acknowledgement

This work was partially supported by the Assistant Secretary for Fossil Energy, Office of Oil, Gas, and Shale Technology of the U. S. Department of Energy, under Contract No. DE-AC03-76SF00098 to the Lawrence Berkeley Laboratory of the University of California. P. Persoff provided invaluable assistance for the experimental program.

Nomenclature

a,b,c	velocity exponents
Ca	capillary number, ratio of viscous to surface tension forces
C_m	mean interfacial radius of curvature
f	wetting-phase relative permeability exponent
g	nonwetting-phase relative permeability exponent
h	film thickness
k	rate constant
k_r	relative permeability
K	permeability
L	length of porous medium
n_f	number density of flowing foam (# of bubbles/volume of flowing foam)
p	phase pressure
PV	pore volume
P_c	capillary pressure, $p_{nw}-p_w$
r	foam generation/coalescence rate (# of bubbles/time/volume of gas)
R	pore radius
S	phase saturation
t	time
u	superficial velocity
U	bubble velocity
v	interstitial velocity
x	spatial variable
X	foam fraction

Greek Letters

α	proportionality constant for effective viscosity
β	trapping parameter in Equation (12)
ϕ	porosity
Π	disjoining pressure
ρ	mass density
σ	equilibrium surface tension
μ	viscosity

Subscripts

l	denotes generation rate constant
-l	denotes coalescence rate constant
b	body
c	coalescence or constriction throat
f	flowing foam
fd	normalized flowing foam saturation
g	gas phase or generation
max	maximum or local maximum
nw	nonwetting phase
rup	rupture
t	trapped foam
T	straight tube
w	wetting phase
wc	connate saturation
wd	normalized wetting-phase saturation

Superscripts

o	scaling or reference value
*	value corresponds to the limiting capillary pressure

Literature Cited

1. Fried, A. N. The Foam Drive Process for Increasing the Recovery of Oil; report 5866, U. S. Dept of Interior, Bureau of Mines, 1961.
2. Hirasaki, G. J. "The Steam Foam Process;" supplement to SPE 19505, available from Soc. Petr. Eng. Book Order Department: Richardson, TX, 1989.
3. Hirasaki, G. J. "The Steam-Foam Process;" J. Petr. Tech., 1989, 41(5), 449-456.
4. Marsden, S. S. Foams in Porous Media - SUPRI TR-49; U.S. D.O.E., July, 1986.
5. Heller, J. P.; Kuntamukkula, M. S. "Critical Review of the Foam Rheology Literature;" Ind. Eng. Chem. Res. 1987, 26(2), 318-25.
6. Baghidikian, S. Y.; Handy, L. L. Transient Behavior of Simultaneous Flow of Gas and Surfactant Solution in Consolidated Porous Media; Topical Report U. S. D.O.E., July, 1991.
7. Rossen, W. R. "Foams in Enhanced Oil Recovery;" in Foams: Theory, Measurements and Applications; Prud'homme, R. K. and Khan. S. Eds.; Marcel Dekker Inc.: New York, to appear.
8. Patzek, T. W. "Description of Foam Flow in Porous Media by the Population Balance Method;" in Surfactant Based Mobility Control Progress in Miscible-Flood Enhanced Oil Recovery;" Smith, D. H. Ed.; ACS Symposium Series No. 373; American Chemical Society: Washington DC, 1988; Ch 16 pp.326-341.
9. Falls, A. H.; Hirasaki, G. J.; Patzek, T. W.; Gauglitz, P. A.; Miller, D. D.; Ratulowski, T. "Development of a Mechanistic Foam Simulator: The Population Balance and Generation by Snap-Off;" Soc. Petr. Eng. Res. Eng. 1988, 3(3), 884-892.
10. Aziz, K.; Settari, A. Petroleum Reservoir Simulation; Applied Science Publishers LTD: London, 1979; p125-199.
11. Hanssen, J. E.; Dalland, M. "Foams for Effective Gas Blockage in the Presence of Crude Oil;" SPE/DOE 20193, presented at SPE 7th Symposium on Enhanced Oil Recovery: Tulsa, OK, April, 1990.
12. Hanssen, J. E.; Haugum, P. "Gas Blockage by Non-Aqueous Foams;" SPE 21002, presented at SPE International Symposium on Oil-Field Chemistry: Anahiem, CA, February, 1991.
13. Clark, H. B.; Pike, M. T.; Rengel, G. L. "The Use of Flurochemical Surfactants in Non-Aqueous Stimulation Fluids;" SPE 7894, presented at SPE International Symposium on Oilfield and Geochemistry: Houston, TX, January, 1979.
14. Holcomb, D. L.; Callaway, R. E.; Curry, L. L. "Foamed Hydrocarbon Stimulation Water Sensitive Formations;" SPE 9033, presented at SPE Rocky Mountain Regional Meeting: Casper, WY, May, 1980.

15. Holm, L. W. "The Mechanisms of Gas and Liquid Flow Through Porous Media in the Presence of Foam;" Soc. Petr. Eng. J. 1968, 8(4), 359-369.
16. Bikerman, J. J. Foams; Springer-Verlag: Berlin, 1973; p 33-64 184-213.
17. Kraynik, A. M. "Foam Flows;" Ann. Rev. Fluid Mech. 1988, 20, 325-357.
18. Hirasaki, G. J.; Lawson, J. B. "Mechanisms of Foam Flow in Porous Media: Apparent Viscosity in Smooth Capillaries;" Soc. Petr. Eng. J. 1985, 25(2), 176-190.
19. Marsden, S. S.; Earlich, J. J. P.; Albrecht, R. A.; David, A. "Use of Foam in Petroleum Operations;" The Proceedings of the 7th World Petroleum Congress: Mexico City; April, 1967, p 235-242.
20. Ettinger, R. A.; Radke, C. J. "Influence of Foam Texture on Steady Foam Flow in Berea Sandstone;" Soc. Petr. Eng. Res. Eng. 1992, 7(1), 83-90.
21. Ettinger, R. A. Foam Flow Resistance in Berea Sandstone M.S. Thesis, University of California, Berkeley 1989.
22. Wardlaw, N. C.; Li, Y.; Forbes, D. "Pore-Throat Size Correlation from Capillary Pressure Curves;" Transport in Porous Media 1987, 2, 597-614.
23. Trienen, R. J.; Brigham, W. E.; Castanier, L. M. Apparent Viscosity Measurements of Surfactant Foam in Porous Media-SUPRI TR-48; Topical Report U. S. D.O.E., October, 1985.
24. Mast, R. F. "Microscopic Behavior of Foam in Porous Media;" SPE 3997, presented at 47th SPE Annual Meeting: San Antonio, TX, October, 1972.
25. Owete, O. S.; Brigham, W. E. "Flow Behavior of Foam: A Porous Micromodel Study;" Soc. Petr. Eng. Res. Eng. 1987, 2(3), 315-323.
26. Chambers, K. T.; Radke, C. J. "Capillary Phenomena in Foam Flow Through Porous Media;" in Interfacial Phenomena in Petroleum Recovery; Morrow, N. R. Ed.; Marcel Dekker Inc.: New York, 1991; Ch. 6 pp 191-255.
27. Chambers, K. T. Pore-Level Basics for Modeling Foam Flow in Porous Media With Randomly Connected Pore Throats M. S. Thesis, University of California, Berkeley, 1990.
28. Hanssen, J. E. "Foam as a Gas-Blocking Agent in Petroleum Reservoirs. I: Empirical Observations and Parametric Study;" Journal of Petroleum Science & Engineering, accepted for publication 1993.
29. Hanssen, J. E. "Foam as a Gas-Blocking Agent in Petroleum Reservoirs. II: Mechanisms of Gas Blockage;" Journal of Petroleum Science & Engineering, accepted for publication 1993.
30. Rossen, W. R.; Zhou, Z. H.; Mamun, C. K. "Modeling Foam Mobility in Porous Media;" SPE 22627, presented at 66th SPE Annual Technical Conference: Dallas, TX, October, 1991.

31. Bernard, G. G.; Holm, L. W. "Effect of Permeability of Porous Media to Gas;" Soc. Petr. Eng. J. 1964, 4(3), 267-274.
32. Bernard, G. G.; Holm, L. W.; Jacobs, W. L. "Effect of Foam on Trapped Gas Saturation and on Permeability of Porous Media to Water;" Soc. Petr. Eng. J. 1965, 5(4), 295-300.
33. Friedmann, F.; Jensen, J. A. "Some Parameters Influencing the Formation and Propagation of Foams in Porous Media;" SPE 15087, presented at the SPE California Regional Meeting: Oakland, CA, April, 1986.
34. Sanchez, J. M.; Schechter, R. S.; Monsalve, A. "The Effect of Trace Quantities of Surfactant on Nitrogen/Water Relative Permeabilities;" SPE 15446, presented at the 61st SPE Annual Technical Conference: New Orleans, LA, October, 1986.
35. Huh, D. G.; Handy, L. L. "Comparison of Steady- and Unsteady-State Flow of Gas and Foaming Solution in Porous Media;" Soc. Petr. Eng. Res. Eng. 1989, 4(1), 77-84.
36. De Vries, A.S.; Wit, K "Rheology of Gas/Water Foam in the Quality Range Relevant to Steam Foam;" Soc. Petr. Eng. Res. Eng. 1990, 5(2), 185-92.
37. Nahid, B. H. Non-Darcy Flow of Gas Through Porous Media in the Prescence of Surface-Active Agents PhD Thesis, University of Southern California, Los Angeles, California, 1971.
38. Gillis, J. V.; Radke, C. J. "A Dual Gas Tracer Technique for Determining Trapped Gas Saturation During Steady Foam Flow in Porous Media;" SPE 20519, presented at the 65th SPE Annual Technical Conference: New Orleans, LA, September, 1990.
39. Friedmann, F.; Chen, W. H.; Gauglitz, P. A. "Experimental and Simulation Study of High-Temperature Foam Displacement in Porous Media;" Soc. Petr. Eng. Res. Eng. 1991, 6(1), 37-45.
40. Flumerfelt, R. W.; Prieditis, J. "Mobility of Foam in Porous Media;" in Surfactant Based Mobility Control Progress in Miscible-Flood Enhanced Oil Recovery;" Smith, D. H. Ed.; ACS Symposium Series No. 373; American Chemical Society: Washington DC, 1988; Ch 15 pp.295-325.
41. Prieditis, J. A Pore Level Investigation of Foam Flow Behavior in Porous Media PhD Thesis, University of Houston, 1988.
42. Rossen, W. R. "Theory of Mobilization Pressure Gradient of Flowing Foams in Porous Media: I. Incompressible Foam;" J. Colloid Interface Sci. 1990, 136(1), 1-16.
43. Rossen, W. R. "Theory of Mobilization Pressure Gradient of Flowing Foams in Porous Media: II. Effect of Compressibility;" J. Colloid Interface Sci. 1990, 136(1), 17-37.

44. Rossen, W. R. "Theory of Mobilization Pressure Gradient of Flowing Foams in Porous Media: III. Asymmetric Lamella Shapes;" J. Colloid Interface Sci. 1990, 136(1), 38-53.
45. Rossen, W. R.; Gauglitz, P. A. "Percolation Theory and Mobilization of Foams in Porous Media," Am. Inst. Chem. Eng. J. 1990, 36(8), 1176-1188.
46. Rossen, W. R. "Minimum Pressure Gradient for Foam Flow in Porous Media: Effect of Interactions With Stationary Lamellae;" J. Colloid Interface Sci. 1990, 139(2), 457-468.
47. de Gennes, P. G. "Conjectures on Foam Mobilization;" Revue De L'Institut Francais Du Petrol 1992, 47(2), 249-254.
48. Falls, A. H.; Musters, J. J.; Ratulowski, J. "The Apparent Viscosity of Foams in Homogeneous Beadpacks;" Soc. Petr. Eng. Res. Eng. 1989, 4(2), 155-164.
49. Marsden, S. S.; Khan, S. A. "The Flow of Foam Through Short Porous Media and Apparent Viscosity Measurements;" Soc. Petr. Eng. J. 1966, 6(1), 17-25 .
50. Heller, J. P.; Lien, C. L.; Kuntamukkula, M. S. "Foam-Like Dispersion for Mobility Control in CO2 Flood;" SPE 11233, presented at the 57th SPE Annual Technical Conference, New Orleans, LA, September, 1982.
51. Bretherton, F. P. "The Motion of Long Bubbles in Tubes;" J. Fluid Mech. 1961, 10, 166-188.
52. Wong, H. The Motion of a Long Bubble in Polygonal Capillaries at Low Capillary Numbers PhD Thesis, University of California at Berkeley, Berkeley, California 1992.
53. Stone, H. L. "Probability Model for Estimating Three-Phase Relative Permeability;" J. Petr. Tech. 1970, 22(2), 214-218.
54. Roof, J. G. "Snap-Off of Oil Droplets in Water-Wet Pores;" J. Petr. Tech. 1970, 22, 85-90.
55. Jiménez, A. I.; Radke, C. J. "Dynamic Stability of Foam Lamellae Flowing Through a Periodically Constricted Pore;" in Oil-Field Chemistry: Enhanced Recovery and Production Stimulation; Borchardt, J. K.; Yen, T. F. Eds.; ACS Symposium Series No. 396, American Chemical Society: Washington D.C., 1989; Ch 25 pp 460 - 479.
56. Kanda, M.; Schechter, R. S. "On the Mechanism of Foam Formation in Porous Media;" SPE 6200, presented at the 51st SPE Annual Technical Conference: New Orleans, LA, October, 1976.
57. Li, Y.; Wardlaw, N. C. "The Influence of Wettability and Critical Pore-Throat Size Ratio on Snap-Off;" J. Colloid Interface Sci., 1986, 109(2), 461-472.
58. Sanchez, J. M.; Hazlett, R. D. "Foam Flow Through an Oil-Wet Porous Medium: A Laboratory Study;" Soc. Petr. Eng. Res. Eng., 1992, 7(1), 91-97.

59. Gauglitz, P. A. "Coalescence During Division: A Mechanism of Lamellae Rupture in Porous Media;" presented at the AIChE Annual Meeting: Chicago, IL, November 1990.
60. Ransohoff, T. C.; Radke, C. J. "Mechanisms of Foam Generation in Glass-Bead Packs;" Soc. Petr. Eng. Res. Eng. 1988, 3(2), 573-585.
61. Persoff, P.; Radke, C. J.; Pruess, K.; Benson, S. M.; Witherspoon, P. A. "A Laboratory Investigation of Foam Flow in Sandstone at Elevated Pressure;" Soc. Petr. Eng. Res. Eng. 1991, 6(3), 365-371.
62. Khatib, Z. I.; Hirasaki, G. J.; Falls, A. H. "Effects of Capillary Pressure on Coalescence and Phase Mobilities in Foams Flowing Through Porous Media;" Soc. Petr. Eng. Res. Eng. 1988, 3(3), 919-926.
63. Derjaguin, B. V.; Obukhov, E. V. "Anomalien dünner Flüssigkeitsschichten III;" Acta Physicochim. URSS 1936, 5(1), 1-22.
64. Derjaguin, B. V.; Kussakov, M. M. "Anomalous Properties of Thin Polymolecular Films V.;" Acta Physicochim. URSS 1939, 10(1), 25-44.
65. Bergeron, V.; Radke, C. J. "Equilibrium Measurements of Oscillatory Disjoining Pressure;" Langmuir 1992, 8, 3020-3026.
66. Exerowa, D.R.; Kolarov, T.; Khristov, KHR. "Direct Measurement of Disjoining Pressure in Black Foam Films I. Films from an Ionic Surfactant;" Colloids and Surfaces 1987, 22, 171-185.
67. Derjaguin, B. V.; Kussakov, M. M. "Anomalous Properties of Thin Polymolecular Films V.;" Acta Physicochim. URSS 1939, 10(2), 153-174.
68. Derjaguin, B. V.; Churaev; Muller, V. M. Surface Forces; Consultants Bureau: New York, 1987; pp 25-52, 327-367.
69. Hirasaki, G. J. "Thermodynamics of Thin Films and Three-Phase Contact Angles;" in Interfacial Phenomena in Petroleum Recovery; Morrow, N. R. Ed.; Marcel Dekker Inc.: New York, 1990; Ch. 2 pp 23-76.
70. Khristov, KHR. ; Krugljakov, P.; Exerowa, D R. "Influence of the Pressure in the Plateau-Gibbs Borders on the Drainage and the Foam;" Colloid and Polymer Sci. 1979, 257, 506-511.
71. Khristov, KHR.; Exerowa, D. R ; Krugljakov, P. M. "Influence of Film Type on Foam Stability;" Colloid J. USSR. 1981, 43, 80-84.
72. Vrij, A. "Possible Mechanism for the Spontaneous Rupture of Thin, Free Liquid Films;" Disc. Faraday Soc. 1966, 42, 23-33.
73. Leverett, M. C. "Capillary Behavior in Porous Solids;" Trans AIME 1941, 195, 159-172.
74. Jiménez-Laguna, A. I. Stability of Thin Liquid Films: Theory and Application to Foam Flow in Porous Media PhD Thesis University of California at Berkeley, Berkeley, California 1991.

75. Huh., D. G.; Cochrane, T. D.; Kovarik, F. S. "The Effect of Microstructure Heterogeneity on CO₂/Foam Mobility. Part 1: A Mechanistic Study;" J. Petr. Tech. 1989, 41, 872-879.
76. Aronson, A. S.; Bergeron, V.; Fagan, M. E.; Radke, C.J. "The Influence of Disjoining Pressure on Foam Stability and Flow in Porous Media;" Colloids and Surfaces, to appear.
77. Osterloh, W. T.; Jante, M. J. Jr. "Effects of Gas and Liquid Velocity on Steady-State Foam Flow at High Temperature;" SPE/DOE 24179, presented at 8th SPE/DOE Symposium on Enhanced Oil Recovery, Tulsa, OK, April, 1992.
78. Kavscek, A. R.; Radke, C. J. "A Comprehensive Description of Transient Foam Flow in Porous Media;" No. FS-9, presented at DOE/NIPER Field Application of Foams for Oil Production Symposium: Bakersfield, CA, February 1993.
79. Kavscek, A. R.; Patzek, T. W.; Radke, C. J. "Simulation of Foam Displacement in Porous Media;" SPE 26402, presented at 68th SPE Annual Technical Conference: Houston, TX, October, 1993.
80. Kavscek, A. R. PhD thesis, University of California at Berkeley, Berkeley, California, in preparation 1993.
81. Lee, H. O.; Heller, J. P. "Laboratory Measurements of CO₂-Foam Mobility;" Soc. Petr. Eng. Res. Eng. 1990, 5(2), 193-197.
82. Zhou, Z.; Rossen, W. R. "Applying Fractional Flow Theory to Foam Processes at the 'Limiting Capillary Pressure;" SPE /DOE 24180, presented at the SPE/DOE 8th Symposium on Enhanced Oil Recovery: Tulsa, OK, April, 1992.
83. Chang, S. H.; Owusu, L. A.; French, S. B.; Kovarik, F. S. "The Effect of Microscopic Heterogeneity on CO₂-Foam Mobility: Part 2--Mechanistic Foam Simulation;" SPE/DOE 20191, presented at the 7th SPE/DOE Symposium on Enhanced Oil Recovery: Tulsa, OK, April, 1990.
84. Chou, S. I. "Percolation Theory of Foam in Porous Media;" SPE/DOE 20239, presented at th 7th SPE/DOE Symposium on Enhanced Oil Recovery: Tulsa, OK, April, 1990.
85. Fisher, A. W.; Foulser, R. W. S.; Goodyear, S. G. "Mathematical Modeling of Foam Flooding;" SPE/DOE 20195, presented at SPE/DOE 7th Symposium on Enhanced Oil Recovery: Tulsa, OK, April, 1990.
86. Liu, D.; Brigham, W. E. "Transient Foam Flow in Porous Media with Cat Scanner;" Topical Report U.S. D.O.E., March, 1992.
87. Patzek, T. W.; Koinis, M. T. "Kern River Steam-Foam Pilots;" J. Petr. Tech. 1990, 42(4), 496-503.
88. Patzek, T. W.; Myhill, N. A. "Simulation of the Bishop Steam Foam Pilot;" SPE 18786, presented at SPE California Regional Meeting: Bakersfield, CA, April 1989.

89. Mohammadi, S. S.; Coombe, D. A. "Characteristics of Steam/Foam Drive Process in Massive Multi-Zone and Thin Single Zone Reservoirs;" SPE 24030, presented at SPE California Regional Meeting: Bakersfield, CA, April 1992.
90. Mohammadi, S. S.; Coombe, D. A.; Stevenson, V. M. "Test of Steam-Foam Process for Mobility Control in S. Casper Creek Reservoir;" Preprint, Paper No. 91-77 Can. Inst. Mining.
91. Marfoe, C. H.; Kazemi, H. "Numerical Simulation of Foam Flow in Porous Media;" SPE 16709, presented at the 62nd SPE Annual Meeting: Dallas, TX, September 1987.
92. Mahmood, S. M.; Tariq, S. M.; Brigham, W. E. "A Model for Prediction of Recovery and Pressure History for 2-D Displacement of Oil Through Porous Media by Gas/Surfactant;" SPE 15076 presented at SPE California Regional Meeting: Oakland, CA, April 1986.
93. Hillestad, J. G.; Mattax, C. C. "Selecting the Numerical Solution Method;" in Reservoir Simulation; Mattax, C. C.; Dalton, R. L. Eds.; SPE Monograph Series Vol. 13 Society of Petroleum Engineers: Richardson, TX, 1990; Ch6 pp 57-73.
94. Ransohoff, T. C.; Gauglitz, P.A.; Radke, C. J. "Snap-Off of Gas Bubbles in Smoothly Constricted Noncircular Capillaries;" AIChE Journal 1987, 33(5), 753-765.
95. Chou, S. I. "Conditions for Generating Foam in Porous Media;" SPE 22628, presented at the 66th SPE Annual Technical Conference: Dallas, TX, October, 1991.
96. Fagan, M. E. The Stability of Foam and Pseudoemulsion Films and Foam Flow Through Glass Beadpacks MS Thesis, University of California at Berkeley, Berkeley, California 1992.
97. Ginley, G. M.; Radke, C. J. "Influence of Soluble Surfactants on the Flow of Long Bubbles Through a Cylindrical Capillary;" in Oil-Field Chemistry: Enhanced Recovery and Production Stimulation, Borchardt, J. K.; Yen, T. F. Eds.; ACS Symposium Series No. 396, American Chemical Society: Washington D.C., 1989; Ch 26 pp 480-501.
98. Corey, A. T. "The Interrelation Between Gas and Oil Relative Permeabilities;" Producer's Monthly 1954, 19(1), 38-41.
99. Yang, S. H.; Reed, R. L. "Mobility Control Using CO₂ Foams;" SPE 19689, presented at the 64th SPE Annual Meeting: San Antonio, TX, October 1989.
100. Minssieux, L. "Oil Displacement by Foams in Relation to Their Physical Properties in Porous Media," J. Petr. Tech. 1974, 26(1), 100-108.

Table 1: Parameter Values

Two-Phase Flow Parameters		Population Balance Parameters	
<u>parameter</u>	<u>value</u>	<u>parameter</u>	<u>value</u>
K	1.3 μm^2	k_1	1.4 E+5 $\text{s}^{1/3} \text{cm}^{-13/3}$
ϕ	0.25	k_{-1}^0	9.0 E-4 cm^{-1}
f	3.0	S_w^*	0.26
k_{rw}^0	0.70	a	0.33
g	3.0	b	1.0
k_{rg}^0	1.0	α	4.0 E-6 $\text{mPa}^{4/3} \text{s}^{8/3} \text{cm}$
S_{wc}	0.25	c	0.33
μ_w	1.0 $\text{mPa} \cdot \text{s}$	$X_{t,\text{max}}$	0.90
μ_g	0.018 $\text{mPa} \cdot \text{s}$	β	1.0 E-3 cm^3

Figure Captions

- Figure 1: Cross-sectional view of cornered pores. Shaded wetting fluid is held in pore corners. (After Ref 26, © 1991 Marcel Dekker Inc.)
- Figure 2: Photomicrograph of foam in a transparent-glass micromodel. A white scale marker at lower left corresponds to 100 μm . The leftmost black arrow marks a large liquid-filled pore connected to the foam flow channel by a small pore throat. The black arrow to the right of center indicates the growth of a wetting collar (after 27).
- Figure 3: Schematic of a continuous-gas foam in porous media. A continuous-gas channel is unshaded and trapped gas is darkly shaded.
- Figure 4: Pore-level schematic of fluid distribution for a discontinuous-gas flowing foam. Flowing bubbles are unshaded and trapped gas is darkly shaded. (After 38, © 1990 SPE-AIME).
- Figure 5: Schematic of snap-off mechanism. Gas is unshaded. (a) Gas entry into liquid filled pore throat, (b) Gas finger and wetting collar formation prior to breakup (c) Liquid lens after snap-off (After 60, © 1989 SPE-AIME).
- Figure 6: Schematic of division mechanism. A lamella is flowing from the left to the right. (a) Gas bubble approaching branch point (b) Divided gas bubbles (After 60, © 1989 SPE-AIME).
- Figure 7: Schematic of leave-behind mechanism. (After Ref 60, © 1989 SPE-AIME)
- Figure 8: Experimental disjoining pressure isotherm at ambient temperature for sodium dodecyl sulfate (0.001 M) in brine (0.18 M NaCl). (After 65, © 1992 American Chemical Society)
- Figure 9: Foam lamella translating from left to right in a periodically constricted tube. Coalescence occurs at t_3 .
- Figure 10: Comparison of foam lamella rupture pressure and beadpack pressure gradient during steady-state foam flow. Upward directed arrows indicate that the actual rupture pressure is greater than the value indicated.
- Figure 11: Schematic of generation and coalescence rate versus aqueous phase saturation. Arrows indicate how generation and coalescence rates change with increasing interstitial velocities.
- Figure 12: Experimental and model transient aqueous phase saturation profiles. Model results are shown with solid lines. Experimental data points (symbols) are connected by dashed lines.
- Figure 13: Experimental and model transient pressure profiles. Model are results shown with solid lines. Experimental data points (symbols) are connected by dashed lines.
- Figure 14: Calculated flowing foam texture.

Figure 15: Experimental and model steady-state pressure drop versus liquid velocity. Gas-phase velocity is held constant. Symbols are experimental data while solid lines are model predictions. Error bars are shown.

Figure 16: Experimental and model steady-state pressure drop versus gas velocity. Aqueous-phase velocity is held constant. Symbols are experimental data while solid lines are model predictions. Error bars are shown.

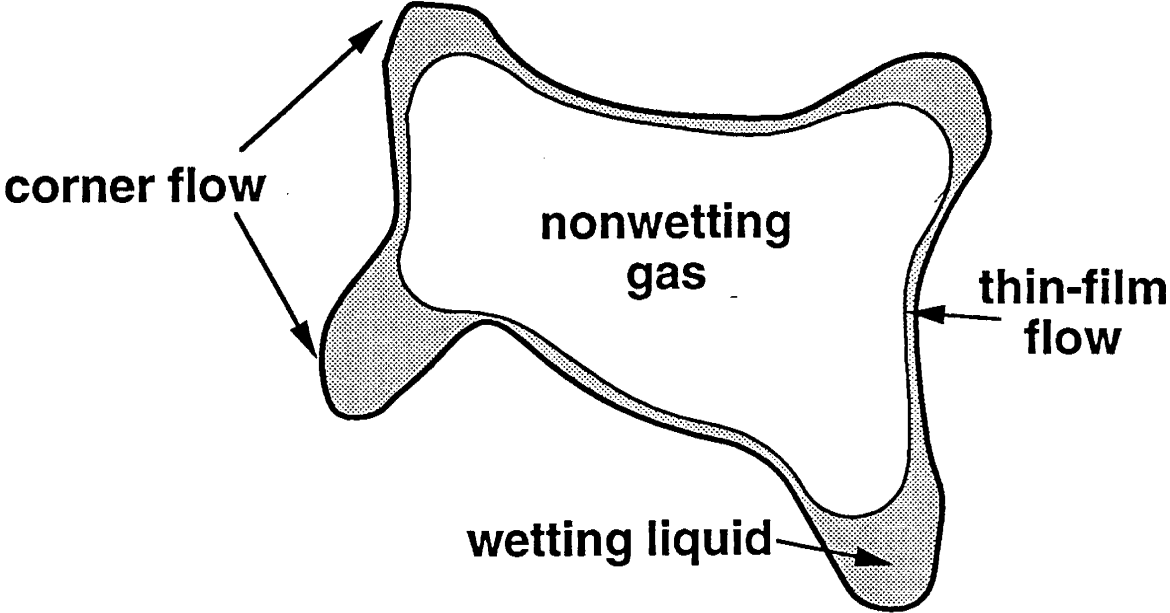


Figure 1



Figure 2

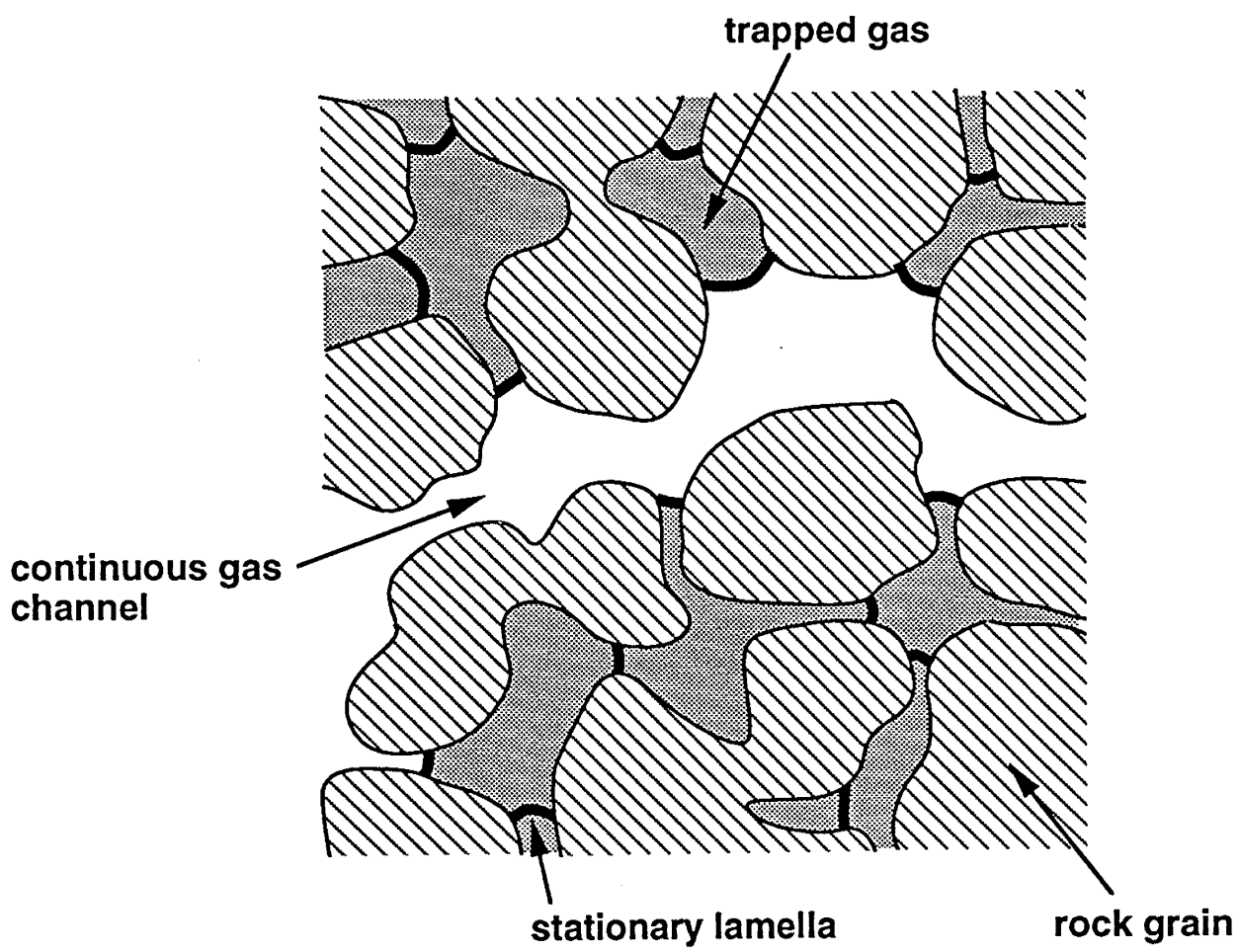
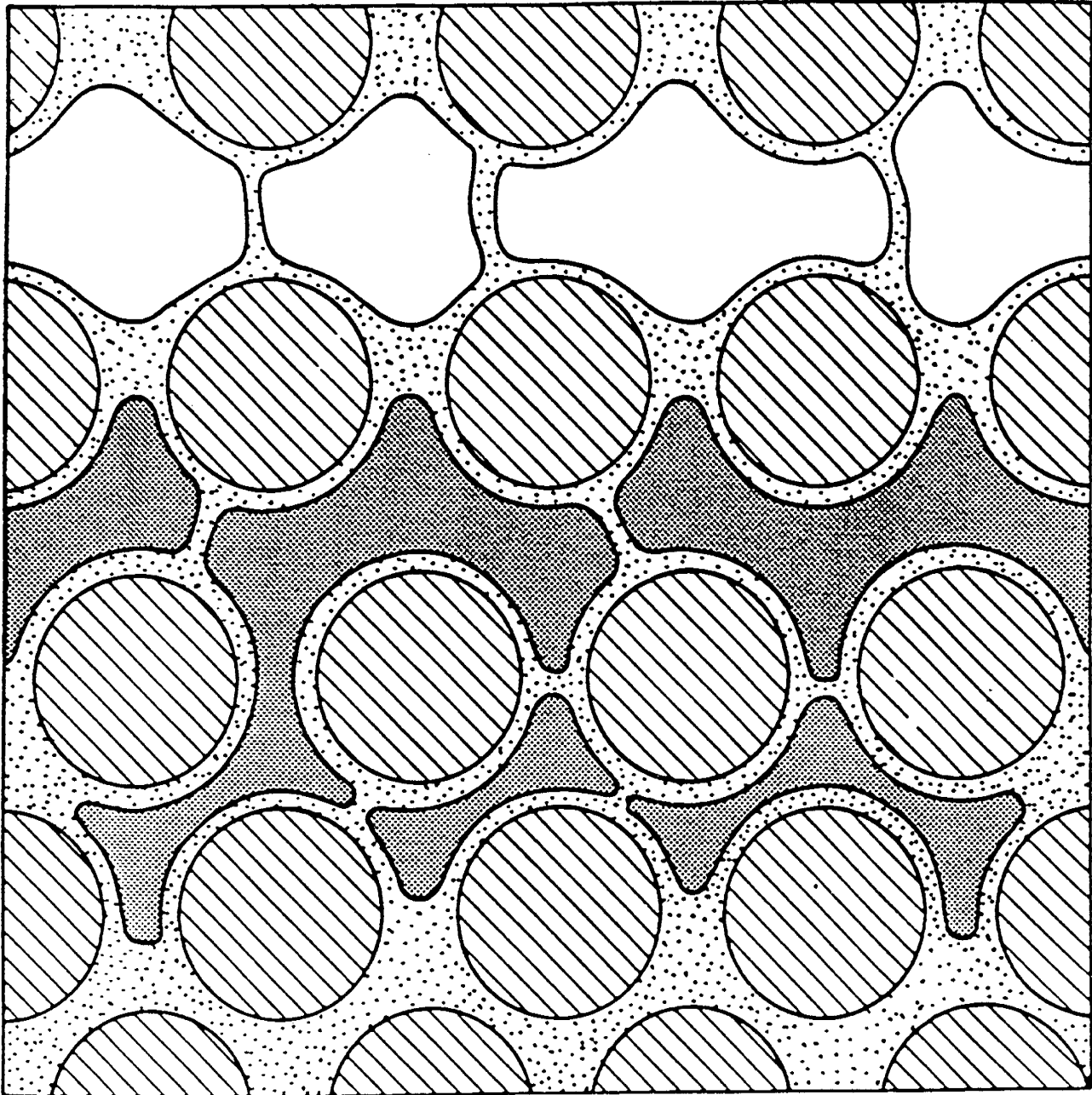


Figure 3



XBL 909-2973

Figure 4

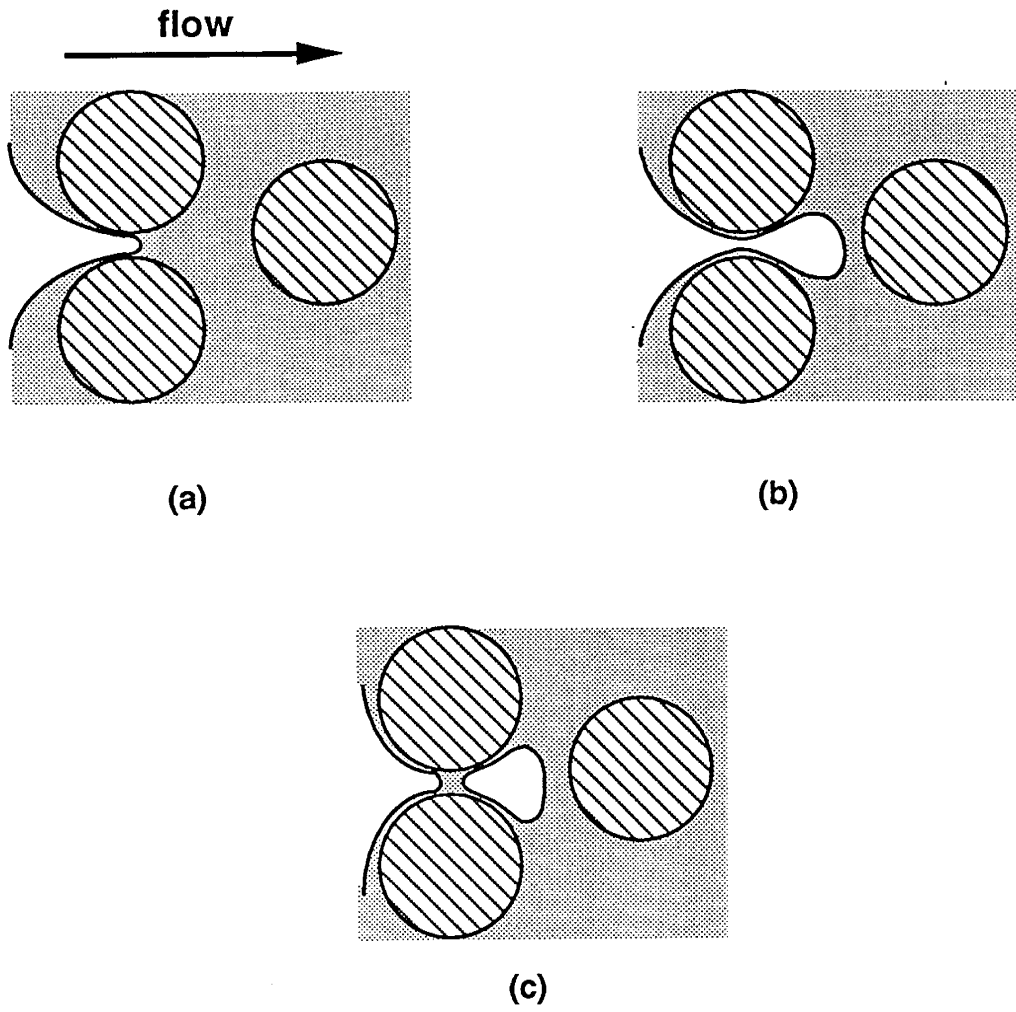
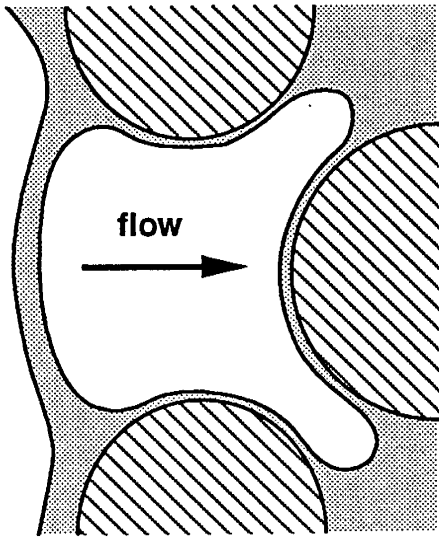
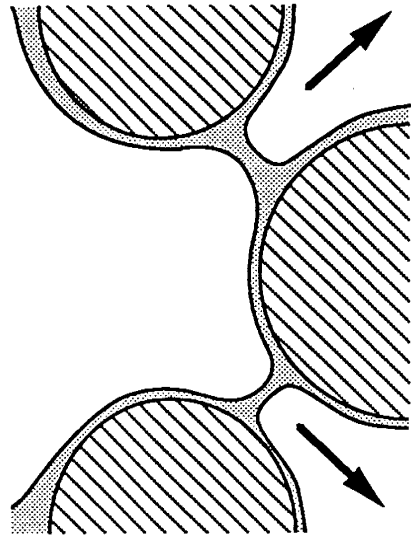


Figure 5



(a)



(b)

Figure 6

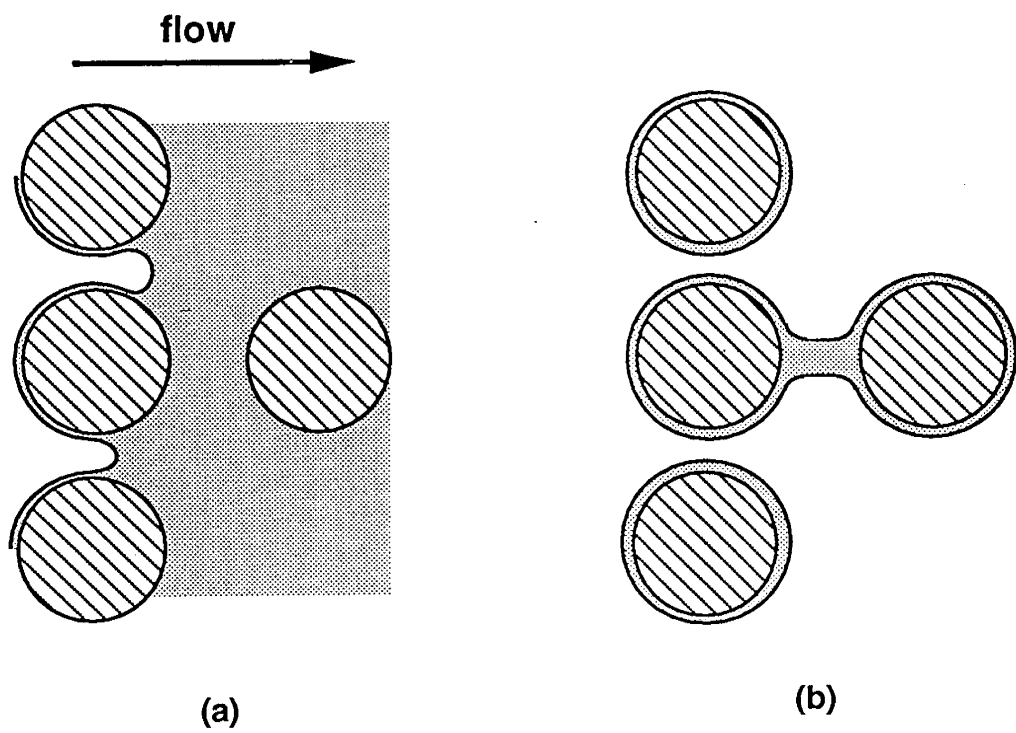


Figure 7

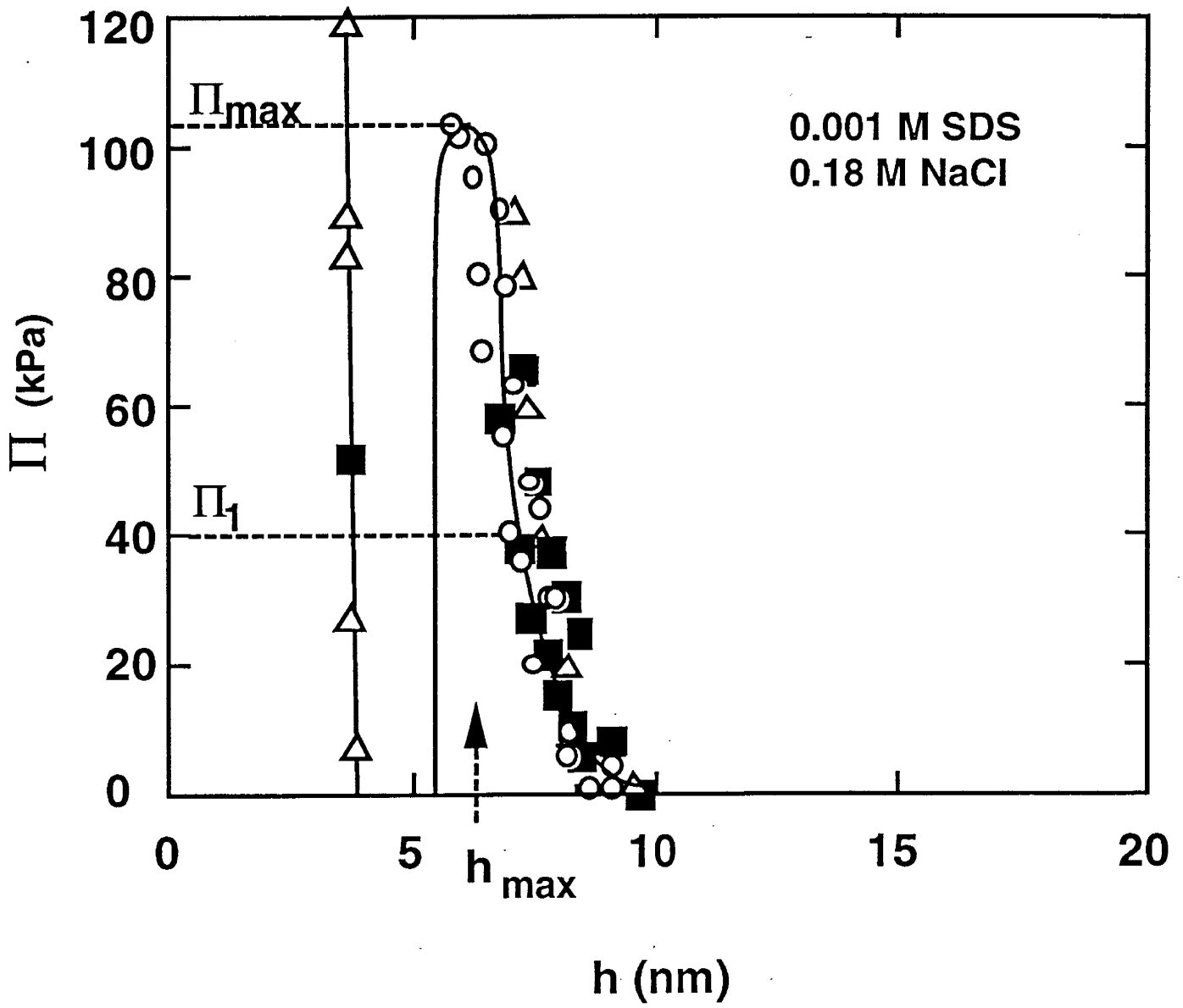


Figure 8

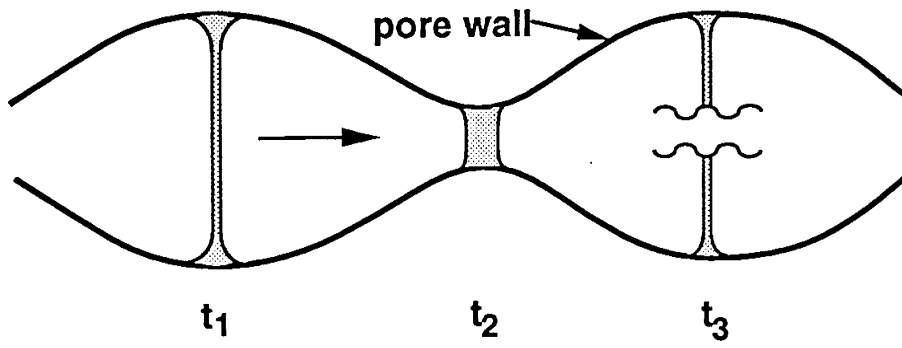


Figure 9

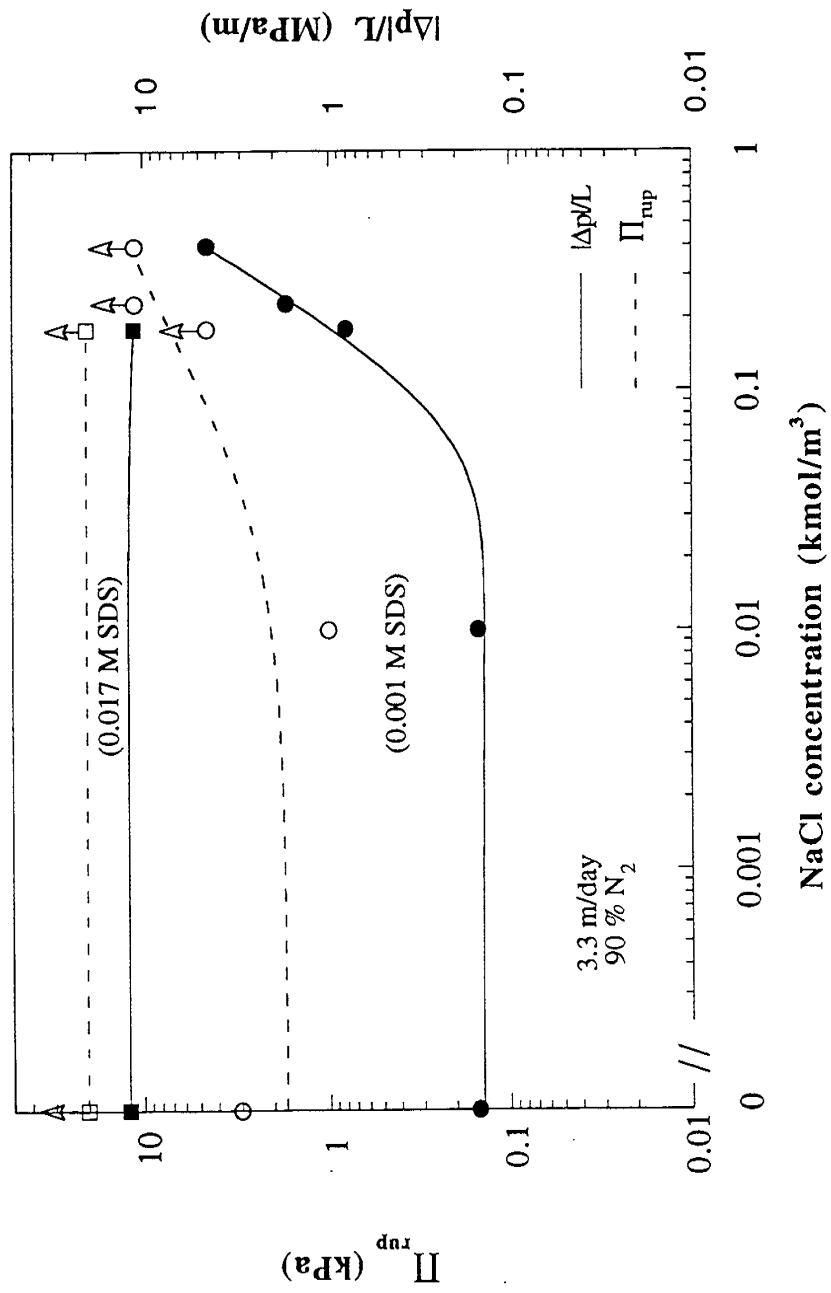


Figure 10

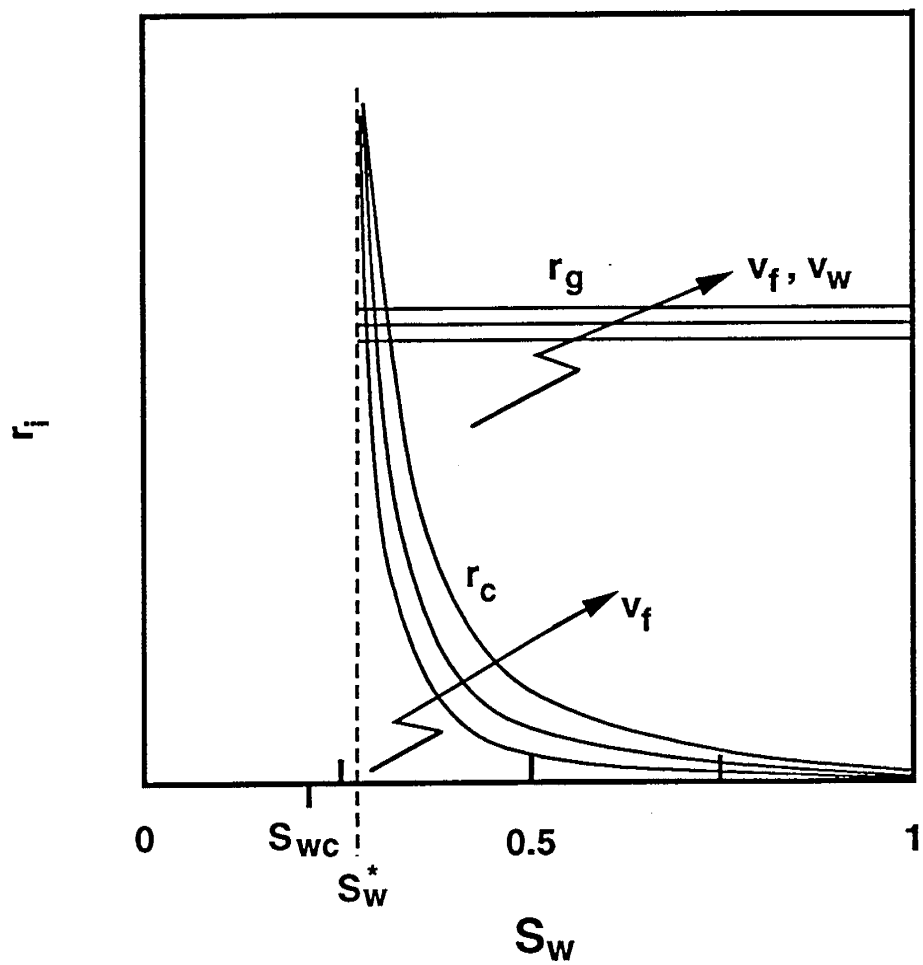


Figure 11

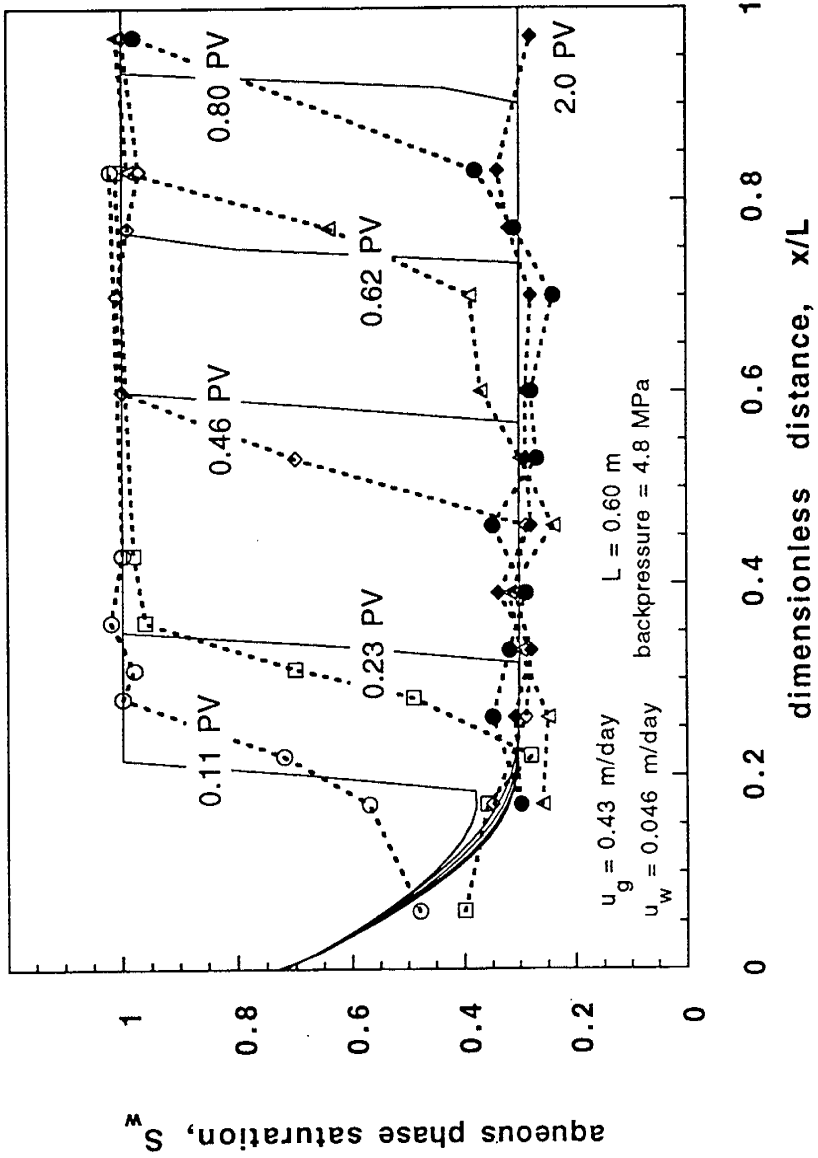


Figure 12

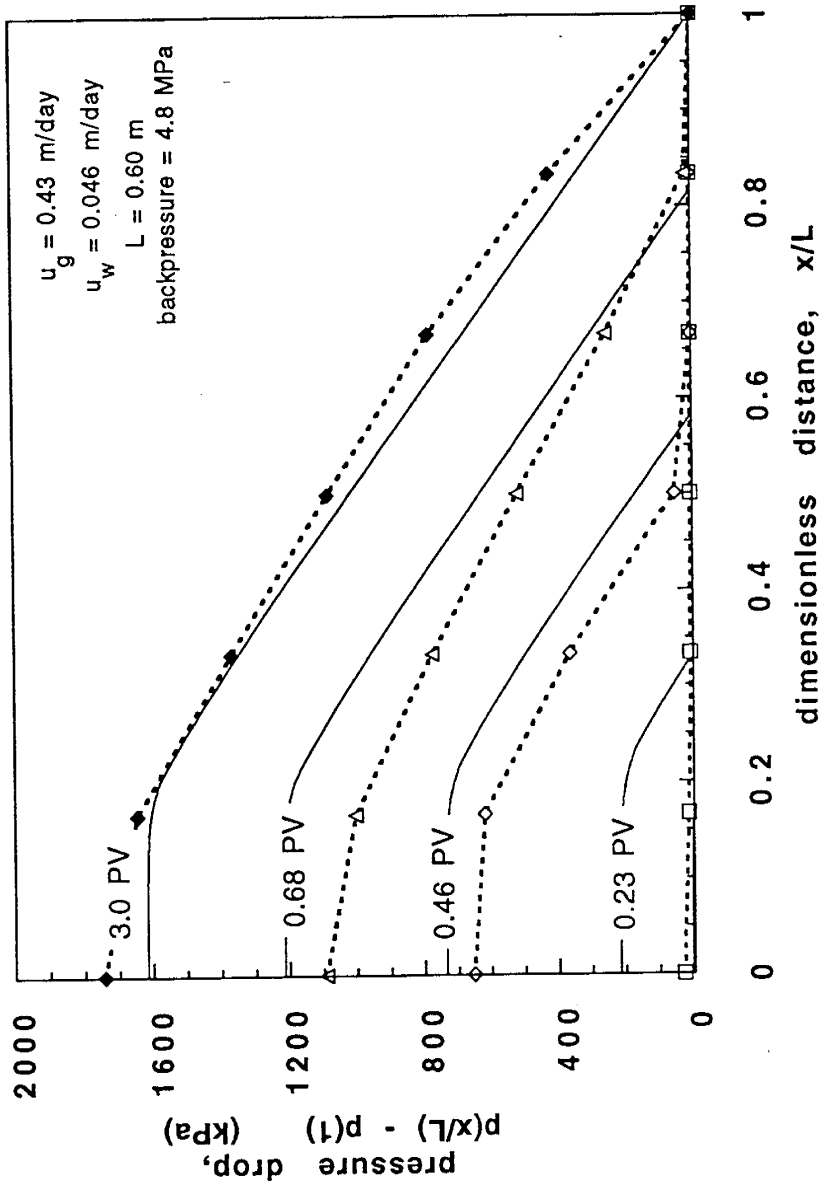


Figure 13

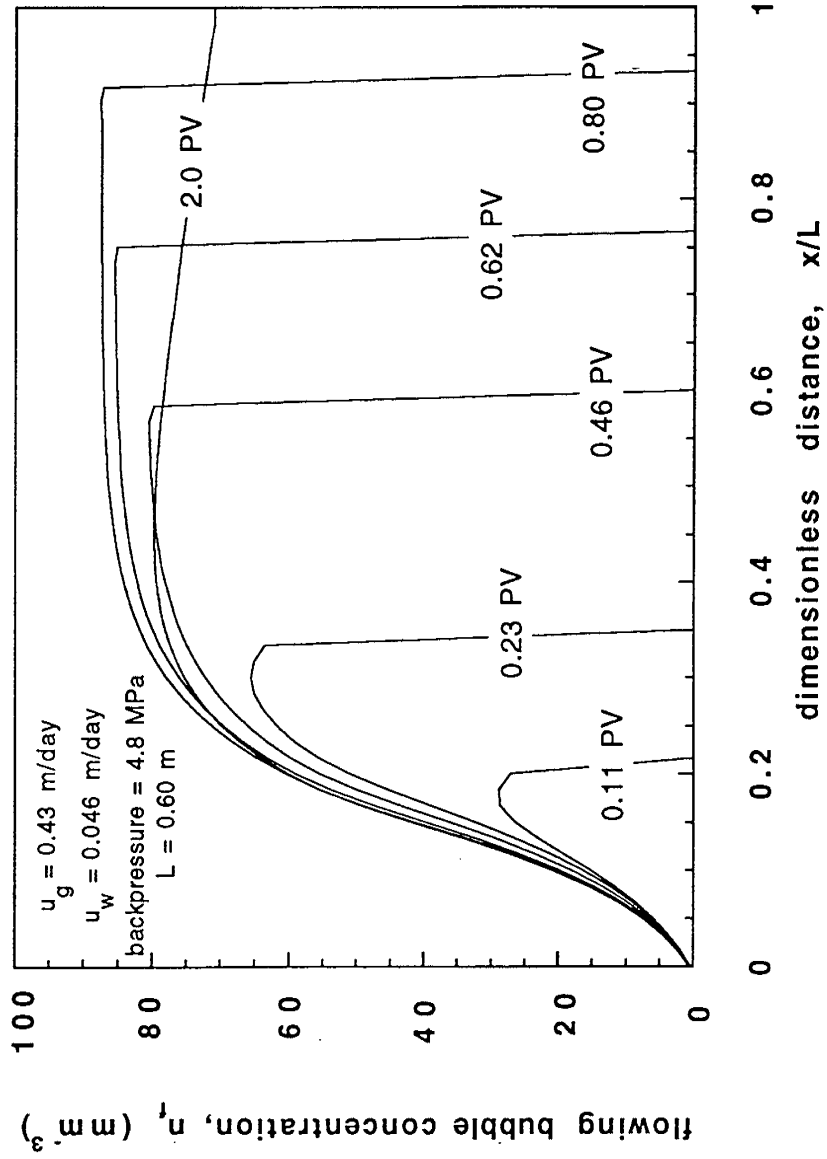


Figure 14

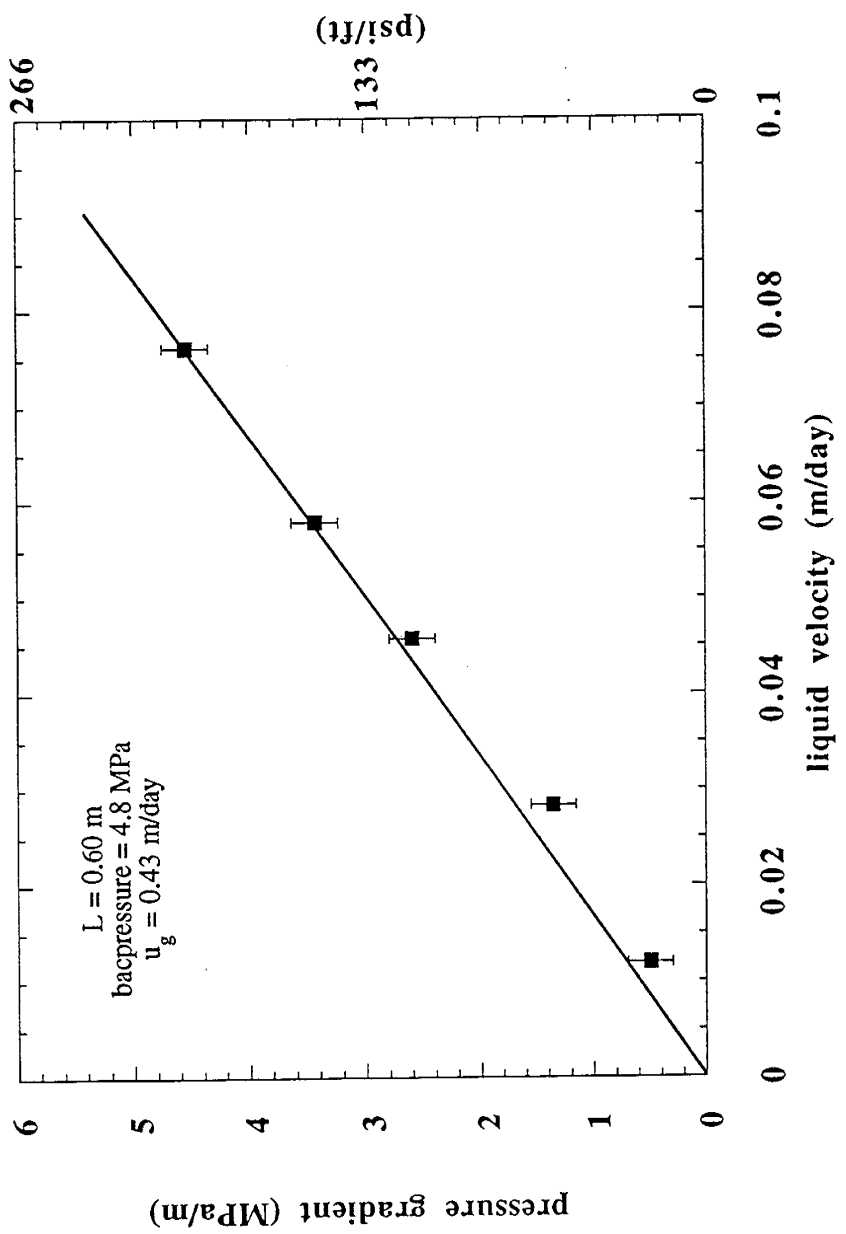


Figure 15

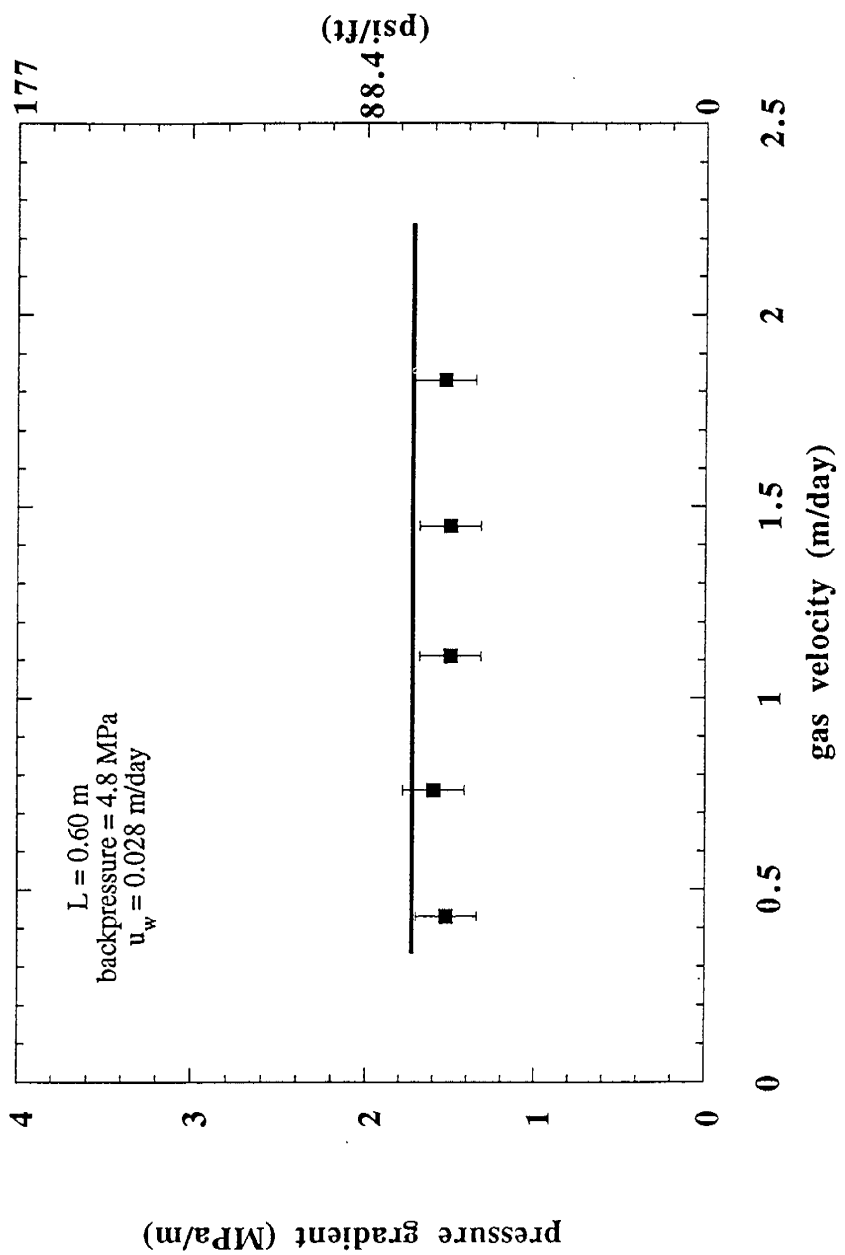


Figure 16

